Intracellular amorphous calcium carbonate biomineralization in methanotrophic gammaproteobacteria was acquired by horizontal gene transfer from cyanobacteria

Running title: ACC biomineralization in aerobic methanotrophs

Benzerara Karim[1], Millet Maxime[1], Skouri-Panet Fériel[1], Gaschignard Geoffroy[1], Mehta Neha[1], Bezard Malo[1], Caumes Geraldine[1], Chevrier Daniel M.[2], Dezi Manuela[1], Duverger Arnaud[1], Guigner Jean-Michel[1], Gutiérrez-Preciado Ana[3], Lefevre Christopher T.[2], López-García Purificación[3], Menguy Nicolas[1], Monteil Caroline L.[2], Pehau-Arnaudet Gerard[4], Penard Esthel[4], Pereiro Eva[5], Scandola Cyril[4], Travert Cynthia[1], Vantelon Delphine[6], Duprat Elodie[1], Callebaut Isabelle[1], Moreira David[3]

[1]Sorbonne Université, Muséum National d'Histoire Naturelle, UMR CNRS 7590. Institut de Minéralogie, de Physique des Matériaux et de Cosmochimie (IMPMC), 75005 Paris, France.

[2]Aix-Marseille Université, CEA, CNRS, BIAM, UMR7265, Institut de Biosciences et Biotechnologies Aix-Marseille, CEA Cadarache, F-13115, Saint-Paul-lez-Durance, France

[3]Unité d'Ecologie Société et Evolution, CNRS, Université Paris-Saclay, AgroParisTech, Gif-sur-Yvette, France

[4]Institut Pasteur, Université Paris Cité, Ultrastructural Bioimaging Unit, 75015 Paris, France

[5]ALBA Synchrotron Light Source, Cerdanyola del Vallés, Barcelona 08290, Spain

[6]Synchrotron SOLEIL, L'Orme des Merisiers, 91190 Saint-Aubin, France

For correspondence: karim.benzerara@sorbonne-universite.fr

Keywords

Amorphous calcium carbonate; methanotrophs; Cyanobacteria; biomineralization; horizontal gene transfer

Abstract

Some bacteria genetically control the biomineralization of intracellular amorphous calcium carbonates (iACC) with potential implications for microbial physiology, evolution, bioremediation and biogeochemical cycling. Until now, this capacity has been documented in *Cyanobacteria*, the giant gammaproteobacterium *Achromatium* and a few magnetotactic *Pseudomonadota* and *Nitrospirota*. Here, we report the discovery of iACC biomineralization in members of the *Methylococcaceae*, a family of aerobic methanotrophic *Gammaproteobacteria*. A homolog of the *ccyA* gene, previously considered a diagnostic marker for iACC formation in *Cyanobacteria*, was identified in several *Methylococcaceae* genomes, based on a search of the conserved C-terminal (GlyZip)3 domain of the encoded calcyanin protein, with a sequence coverage higher than 60% and an E-value lower than $1e^{-20}$. Moreover, two cultivated strains, *Methylococcus geothermalis* and *Methylococcus mesophilus*, whose genomes contained the *ccyA* gene, were consistently shown to form iACC granules. The *ccyA* genes of *Methylococcaceae* and *Microcystis* share higher sequence similarity (47%) than with other *Cyanobacteria* (around 30%) within their common $(GlyZip)_3$ domain, suggesting horizontal gene transfer (HGT) from an ancestral *Microcystis*-like cyanobacterium to *Methylococcaceae*. This finding extends the known taxonomic distribution of *ccyA* and suggests that the capability to biomineralize iACC was acquired by HGT, possibly in environments such as those close to the oxyclines of lakes, where *Cyanobacteria* and *Methylococcaceae* commonly co-exist. The discovery of iACC in methane-oxidizing *Methylococcaceae* highlights a previously unrecognized coupling between calcium carbonate biomineralization and methane cycling in aquatic environments, suggesting that iACC formation may play an overlooked role in microbial carbon storage and local geochemical regulation.

1. Introduction

Many bacteria are capable of forming a wide range of mineral phases through a process known as biomineralization. This process may serve specific biological functions such as protection, detoxification, assistance in cell movements or storage (Cosmidis and Benzerara, 2022) and has a significant impact on both local and global geochemical cycles, inspiring a variety of applications (Qin et al., 2020; Wan et al., 2024; Zhang et al., 2023). Among biomineralizing bacteria, several phylogenetically diverse species have been shown to form intracellular amorphous calcium carbonates (iACC). The giant gammaproteobacterium *Achromatium oxaliferum* was the first such organism discovered, as early as the late 19th century (Schewiakoff, 1893). For a long time, it remained the only known iACC-biomineralizing bacterium (Benzerara et al., 2021; Gray, 2006). However, since 2012, diverse cyanobacteria have also been found to form iACC (Bacchetta et al., 2024; Benzerara et al., 2014, 2022; Couradeau et al., 2012). More recently, additional members of the *Pseudomonadota* and *Nitrospirota*, including magnetotactic bacteria capable of biomineralizing intracellular magnetite crystals (Fe(II)-Fe(III) oxides), have been shown to form iACC as well (Liu et al., 2021, 2025; Mangin et al., 2025; Monteil et al., 2020). This rapidly expanding diversity of iACC-forming bacteria suggests that many more such organisms likely remain to be discovered.

Forming iACC granules incurs an energy cost to cells, at least under certain conditions (Cam et al., 2017), suggesting that these granules likely confer adaptive benefits to the cells. However, their exact biological role remains poorly understood (Cosmidis and Benzerara, 2022). Some studies have proposed that iACC granules may buffer intracellular pH fluctuations, serve as carbon reservoirs, or act as ballast for the cells (Görgen et al., 2020; Monteil et al., 2020). Regardless of their specific function, iACC granules involve a particular Ca homeostasis in the cells that form them, including Ca exchange between the cells and the surrounding solution

with a net inward influx (Benzerara et al., 2023; Mehta et al., 2023, 2024). Studying these granules offers valuable insights: (i) Amorphous calcium carbonate (ACC) is essential to many $CaCO_3$-biomineralizing eukaryotes (Gilbert et al., 2022), and the ability to form iACC may have originated early in evolutionary history within prokaryotes before being transferred to eukaryotes (Ponce-Toledo et al., 2017). Testing this hypothesis requires further exploration of the evolutionary links between iACC formation across different bacterial lineages. (ii) iACC-forming bacteria can influence the local geochemical cycling of alkaline earth metals (Ca, Sr, Ba) and other metals, particularly when they bloom as large populations (Blondeau et al., 2018b; Gaetan et al., 2023; Liu et al., 2025). Last, (iii) some of these bacteria are capable of sequestering toxic radioisotopes, opening new avenues for the development of bioremediation strategies (Mehta et al., 2019, 2022a; Pamart et al., 2025).

Despite the significance of this biomineralization process, the molecular mechanisms underlying bacterial iACC formation remain largely unexplored. In *Cyanobacteria*, iACC forms within envelopes thought to consist of proteins and/or lipid monolayers (Blondeau et al., 2018a). Through comparative genomics, a novel gene family named *ccyA* was identified (Benzerara et al., 2022). This gene family lacks homologs with a known function but serves as a diagnostic marker for iACC formation in *Cyanobacteria*. The *ccyA* gene family encodes two-domain proteins, the calcyanins. The C-terminal domain of calcyanins represents a large part of the full-length proteins and is conserved across cyanobacterial clades. It is composed of several long glycine zipper (Gly-zip) motifs. In contrast, the N-terminal domain is much shorter and variable, defining four distinct calcyanin subgroups, corresponding to different *Cyanobacteria* clades (Benzerara et al., 2022). Overall, it is the conserved C-terminal domain that allows to confidently identify members of the calcyanin family despite the variability of their N-terminal domains. A strong correlation has been established between the presence of the C-terminal domain and the capability of a cyanobacterium to form iACC. Interestingly, the

103 N-terminal domain of one calcyanin subgroup contains a CoBaHMA domain, which is
104 hypothesized to play a regulatory role, possibly interacting with anionic lipids (Gaschignard et
105 al., 2024). Furthermore, a recent study suggests that other genes may operate in concert with
106 *ccyA*, such as a *cax* gene encoding a Ca^{2+}/H^{+} transporter (Bruley et al., 2025).

107 In this study, we report the discovery of a homolog of the *ccyA* gene in *Methylococcaceae*, a
108 family of *Gammaproteobacteria*. Furthermore, the two available cultivated strains from this
109 family were found to form iACC, providing evidence that *ccyA* is a marker of iACC
110 biomineralization beyond the phylum *Cyanobacteria*. The phylogenetic distribution of *ccyA*
111 within *Methylococcales*, along with its comparison with the *ccyA* genes in *Cyanobacteria*, offer
112 new insights into the evolutionary origins of iACC biomineralization in *Methylococcaceae*.

113

114 ## 2. Materials and methods

115 ### 2.1 Genome collection and phylogenomic analyses

116 The 858 high-quality genome sequences of species of the order *Methyloccoccales* available in
117 the Genome Taxonomy Database (GTDB) version r220 (Parks et al., 2022) were downloaded.
118 They included seven families according to the GTDB taxonomy: *Cycloclasticaceae* (43
119 genomes), *Methylococcaceae* (112 genomes), *Methylomonadaceae* (679 genomes),
120 *Methylothermaceae* (13 genomes), UBA1147 (6 genomes), UBA2778 (3 genomes), and
121 DRLZ01 (2 genomes). Eight additional gammaproteobacterial genomes were downloaded to
122 serve as outgroup in phylogenomic analyses: *Coxiella burnetii* cb109 (GCA_000300315.1),
123 *Legionella pneumophila* Hextuple_2q (GCA_000277025.1), *Reinekea blandensis* MED297
124 (GCF_000153185.1), *Dichelobacter nodosus* (GCF_001263335), *Francisella tularensis*
125 FSC147 (GCA_000018925.1), *Nitrosococcus oceani* ATCC 19707 (GCF_000012805.1),
126 *Halorhodospira* sp. (GCA_007121755.1), and *Alkalilimnicola ehrlichii* MLHE-1

127 (GCF_000014785.1). Protein-coding genes were predicted with Prodigal (Hyatt et al., 2010)
128 when annotations were missing.
129 GTDB-Tk (Chaumeil et al., 2022) was used to identify 120 conserved protein markers encoded
130 in the whole collection of *Methylococcales* and outgroup genome sequences. Individual
131 markers were aligned using MAFFT L-INS-I v7.310 (Katoh et al., 2019). Poorly aligned sites
132 were removed using trimAl (Capella-Gutiérrez et al., 2009) with the –strictplus option and the
133 resulting trimmed alignments were concatenated using an in-house Python script, yielding an
134 alignment of 36,916 amino acid sites. A Maximum Likelihood tree based on this supermatrix
135 was inferred using IQ-TREE v3.0.1 (Wong et al., 2025) with the LG+G substitution model (Le
136 and Gascuel, 2008). Branch statistical support was calculated with 1,000 ultrafast bootstrap
137 replicates (Hoang et al., 2018). A tree including only the *Methylococcales* species containing
138 the *ccyA* gene was constructed using the same concatenated markers and the same method
139 described above.
140
141 **2.2 Detection of *ccyA***
142 The detection of *ccyA* was conducted using the in-house tool pCALF (standing for python
143 CALcyanin Finder, https://github.com/K2SOHIGH/pcalf/tree/main), which uses four hidden
144 Markov model (HMM) profiles describing the C-terminal glycine zipper triplication (called the
145 $(GlyZip)_3$ motif), specific of calcyanins in *Cyanobacteria* as explained by Gaschignard et al.
146 (2024). These four HMM profiles describe the whole triplication ($(GlyZip)_3$), as well as each
147 glycine zipper individually (Gly1, Gly2, and Gly3). They were searched against protein
148 sequences using pyHMMER (Larralde and Zeller, 2023). A sequence is classified as calcyanin
149 when it has significant hits against the GlyX3 HMM profile (sequence coverage threshold:
150 60%; E-value threshold: $1e^{-20}$) and against individual Gly1, Gly2, and Gly3 HHM profiles in
151 this specific order (sequence coverage threshold: 70%, E-value threshold: $1e^{-10}$).

152

153 **2.3 Sequence and three-dimensional (3D) structure analysis**

154 Calcyanin protein sequences detected in *Methylococcales* were compared with those found in
155 *Cyanobacteria*. For this purpose, multiple sequence alignments were performed using MAFFT
156 L-INS-I v7.310 (Katoh et al., 2019), then checked and further analyzed using Hydrophobic
157 Cluster Analysis (HCA) (Bitard-Feildel et al., 2018). Aligned sequences were rendered on the
158 basis of ESPript 3.0 results (Gouet et al., 2003). 3D structure predictions were performed using
159 the AlphaFold3 server (Abramson et al., 2024). Visualization and manipulation of 3D structures
160 were performed using Chimera 1.13.1 (Pettersen et al., 2004). 3D structure similarities were
161 also explored and quantified using TM-align on the RCSB pairwise structure alignment tool
162 (https://www.rcsb.org/alignment; Bittrich et al., 2024).

163

164 **2.4 Bacterial strains**

165 The strain *Methylococcus geothermalis* IM1 (=JCM 33941 =KCTC 72677) was ordered from
166 the Riken bioresource research center in Japan (https://www.jcm.riken.jp/cgi-
167 bin/jcm/jcm_number?JCM=33941. *M. geothermalis* is an aerobic, planktonic and non-motile
168 methanotroph isolated from a hot spring soil in Korea (Awala et al., 2020). Here, it was cultured
169 in triplicates at 37 °C in 10 mL of modified nitrate mineral salts medium-2 (M1221;
170 https://www.jcm.riken.jp/cgi-bin/jcm/jcm_grmd?GRMD=1221) in a 120-mL glass serum
171 bottle with a 25-75 vol% of CH_4-air mix in the headspace. The genome sequence is available
172 under NCBI accession number CP046565.1.

173 The strain *Methylococcus mesophilus* 16-5^T (=KCTC 82050^T) was provided by Dr. Samuel
174 Imisi Awala from University of Calgary. *M. mesophilus* is a mesophilic, aerobic methanotroph
175 isolated from a rice field in Korea (Awala et al., 2023). It was cultured in triplicates at 21°C in
176 10 mL of modified nitrate mineral salts medium-2 (M1221; https://www.jcm.riken.jp/cgi-

177 bin/jcm/jcm_grmd?GRMD=1221) in a 120-mL glass serum bottle with a 25-75 vol% of CH_4-
178 air mix in the headspace. The genome sequence is available under NCBI accession number
179 CP110921.1.
180 Cell growth for both strains was assessed by measuring optical density at 600 nm. The pH of
181 the cell suspension was measured over the growth of the cells with a precision better than 0.1.
182
183 **2.5 Fourier Transform infrared spectroscopy (FTIR)**
184 FTIR spectroscopy analyses of both strains were performed to detect bulk signals from iACC
185 inclusions, following the methodology outlined by (Mehta et al., 2022b). Cells were pelleted
186 from 15 mL of a culture grown to an optical density of 0.2, washed with MilliQ® water, dried
187 and ground in an agate mortar. Attenuated total reflectance Fourier transform infrared (ATR-
188 FTIR) spectra were acquired in the mid-IR region (4000–600 cm^{-1}) using a NICOLET 6700
189 FTIR spectrometer equipped with a diamond internal reflection element (IRE), a KBr beam
190 splitter and a deuterated triglycine sulfate (DTGS) detector. Spectra were collected by
191 averaging 64 scans at resolution of 4 cm^{-1}.
192
193 **2.6 Synchrotron-based X-ray absorption near-edge structure (XANES) spectroscopy**
194 The relative quantification of Ca in iACC within *M. geothermalis* cells was achieved using
195 XANES spectroscopy, following the approach detailed by Mehta et al. (2023). For this, 15 mL
196 of a cell suspension were harvested by centrifugation, washed, and dried at 37 °C for 48 hours.
197 The dried biomass (~5 mg) was then diluted in 35 mg cellulose, pressed into a 10 mm diameter
198 pellet, and mounted onto Ca-free holders. XAS at the Ca K-edge was performed on the LUCIA
199 beamline at the SOLEIL synchrotron (Saint-Aubin, France) (Flank et al., 2006; Vantelon et al.,
200 2016). The fixed exit double-crystal monochromator was equipped with Si (111) crystals.
201 Spectra were recorded in the fluorescence mode using a 60 mm^2 mono-element silicon drift
202 diode detector (Bruker). In the pre-edge region (3940–4030 eV), spectra were recorded with a

203 step size of 2 eV and a counting time of 1 s. In the edge region (4030–4070 eV), spectra were
204 recorded with a step size of 0.25 eV and a counting time of 1 s. The sample holder was
205 positioned at a 24° angle relative to the fluorescence detector to minimize self-absorption
206 effects and was maintained at a temperature of 77 K using a liquid He-cryostat to minimize
207 potential beam damages and localized heating. Energy calibration was performed using a calcite
208 reference, with the first inflection point set to 4045 eV.
209
210 **2.7 Scanning electron microscopy (SEM)**
211 Cell suspensions of both *M. geothermalis* and *M. mesophilus* were filtered onto 0.22 µm Isopore
212 polycarbonate filters and rinsed with 10 mL of MilliQ® water. The filters were air-dried at
213 ambient temperature and mounted on aluminum stubs using double-sided carbon tape. Before
214 analysis, the filters were coated with a thin layer of carbon via evaporation to make them
215 electrically conductive. Scanning electron microscopy (SEM) analyses were performed using a
216 Zeiss™Ultra55 SEM with an electron accelerating voltage of 10 kV, a working distance of 7.5
217 mm and a 60 µm aperture. Images were captured using a backscattered electron detector (AsB
218 detector). Energy-dispersive X-ray spectrometry (EDXS) data were acquired with a Bruker
219 QUANTAX EDS detector, enabling hyperspectral imaging (HyperMap), and the data were
220 analysed with the Esprit software (Brucker).
221
222 **2.8 Transmission electron microscopy**
223 A 0.5 mL cell suspension was harvested by centrifugation, rinsed twice in 1 mL of MilliQ®
224 water before resuspension in 0.5 mL of MilliQ® water. A drop of 3 µL was deposited onto a
225 formvar-coated TEM grid and air-dried. Observations were carried out using a Jeol 2100F TEM
226 microscope operating at 200 kV, equipped with a Schottky emitter, a STEM device for Z-
227 contrast imaging in high-angular annular dark-field (HAADF) mode, and a Jeol Si(Li) X-ray
228 detector for elemental analyses via energy dispersive x-ray spectrometry (EDXS).

229

230 **2.9 Synchrotron-based cryo-soft X-ray tomography (c-SXT)**

231 Three-dimensional X-ray imaging of *M. geothermalis* cells was performed at the ALBA
232 synchrotron (Barcelona, Spain) using cryo-transmission X-ray microscopy at the MISTRAL
233 beamline (Sorrentino et al., 2015). The cryofixation process involved plunge-freezing at the
234 Institut Pasteur (Paris, France) using a Leica EM GP. A Quantifoil TEM grid (Q-R2/1-C2100)
235 was loaded in the chamber of the plunge freezer. Four microliters of a two-day-old *M.*
236 *geothermalis* culture (OD = 0.251) and one microliter of a 100-nm gold nanoparticles
237 suspension (BBI Solutions, 5X concentrated) were deposited on the front of the grid. After
238 blotting for four seconds from the back, grids were plunged into a container filled with liquid
239 ethane cooled with liquid nitrogen (-196°C), ensuring proper vitrification of the samples.
240 Subsequently, the samples were shipped from Paris to the ALBA synchrotron in a dry shipper
241 and transferred to the cryo-chamber of the Mistral beamline for imaging.

242 A tilt series of projections was collected from −70° to +70° in 1° increments (except otherwise
243 mentioned), with an incident X-ray energy of 520 eV. Each projection was exposed for 3
244 seconds. A 40-nm Fresnel zone plate was used, achieving an effective pixel size of 12 nm. The
245 projections were normalized for incoming flux and deconvolved using the measured point
246 spread function of the optical system (Otón et al., 2016). Projections were aligned using Etomo
247 with the 100-nm gold nanoparticle fiducials. Tomographic reconstruction, along with
248 simultaneous iterations reconstruction technique (SIRT) deconvolution, were performed using
249 IMOD (Otón et al., 2016). Volume segmentation, calculations and visualization of tomograms
250 were carried out using the Microscopy Image Browser and ImageJ (Belevich et al., 2016).

251

252

253 **3. Results**

254

255 **3.1 Detection and phylogenetic distribution of *ccyA* in the order *Methylococcales***

256 The *ccyA* gene (more precisely, the long C-terminal domain of the encoded calcyanin protein)
257 has been identified as a diagnostic marker for iACC biomineralization in *Cyanobacteria*.
258 Moreover, homologs of *ccyA*, identified based on the sequence of the calcyanin C-terminal
259 domain, were also reported in four gammaproteobacteria of the order *Methylococcales* in a
260 previous study (Benzerara et al., 2022)). However, the evolutionary relationship between the
261 *ccyA* genes of cyanobacteria and those of *Methylococcales* remains unclear. Furthermore, it is
262 unknown whether *Methylococcales* possessing *ccyA* are capable of forming iACC, as
263 cyanobacteria do. To investigate these questions further, we systematically searched for *ccyA*
264 homologs across the 858 genome sequences of *Methylococcales* species available in the
265 Genome Taxonomy Database (GTDB) version r220 (Parks et al., 2022) (Table S1). This search
266 was performed using the pCALF tool (see Materials and methods) with the E-value, coverage
267 and identity thresholds provided in Table S2.

268 We detected *ccyA* in 39 genomes of species belonging to the order *Methylococcales* (out of 858
269 available genomes, see Table S1), distributed in the genera *Methylococcus* (including *M.*
270 *geothermalis* and *M. mesophilus*), *Methylospira* (*Candidatus* Methylospira mobilis), and
271 *Methylumidiphilus* (many strains affiliated with *M. alinensis*) (Table 1). According to the GTDB
272 taxonomy, all these species were assigned to the family *Methylococcaceae* (represented by a
273 total of 112 genomes; *ccyA*-containing genomes thus represent 35% of the available
274 *Methylococcaceae* genomes); none were associated with the species-rich *Methylomonadaceae*
275 (679 genomes) or with the other families of the order *Methylococcales* (Figure 1 and Figure
276 S1). From the observed phylogenetic distribution of *ccyA* in *Methylococcaceae*, the most
277 parsimonious scenario thus suggests that *ccyA* appeared in a deep branch of *Methylococcaceae*
278 after the divergence from *Methylomonadaceae* (Figure 1). The species possessing *ccyA* occur
279 in diverse environments, including the water column and sediment of freshwater lakes,

compost, active municipal landfills, and rice field soils (Table 1 and Table S2). In all identified genomes, the protein calcyanin was consistently annotated as a hypothetical protein. According to the GTDB metadata, most of the genomes containing *ccyA* (34 out of 39) were metagenome-assembled genomes (MAGs), and only five originated from cultured isolates (Table 1). Only two of these isolates were available: *Methylococcus geothermalis* IM1 and *Methylococcus mesophilus* 16-5, which we further studied to search for their capability to biomineralize iACC.

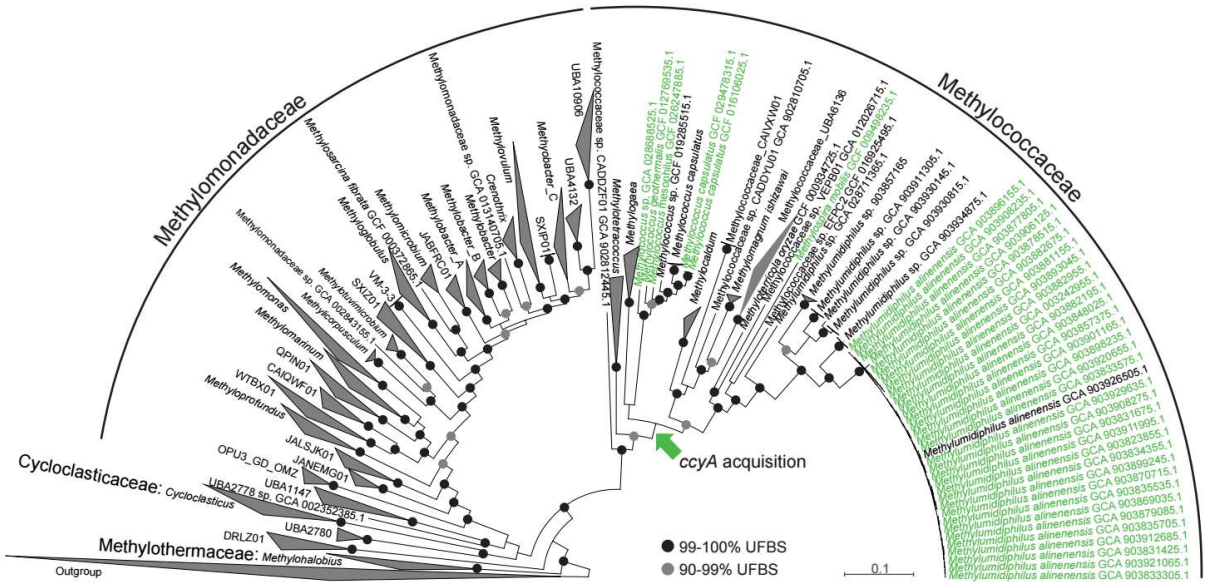

Figure 1: Maximum likelihood phylogenomic tree of 858 *Methylobacterales* taxa available in the Genome Taxonomy Database (GTDB version 220) (see Table S1). The tree is based on the concatenation of 120 conserved proteins. Taxa containing the *ccyA* gene are highlighted in green. Taxa that do not contain the *ccyA* gene are collapsed. Taxon names correspond to the GTDB taxonomy. The green arrow indicates the most likely point (based on maximum parsimony) for the acquisition of *ccyA* by an ancestor of several *Methylococcaceae* lineages (earlier acquisitions would imply an increasing number of subsequent independent losses). Ultrafast bootstrap support (UFBS) values >90% are indicated on branches (black dots: 99-100%; gray dots: 90-99%). The complete, un-collapsed tree is available in Fig. S1.

Genome ID	Environmental biome	GTDB genus	Type	Bibliography
GCF_012769535.1	Geothermal environment	*Methylococcus*	Isolate	Awala SI et al (2020)
GCF_016106025.1	Compost from a depth of 5 cm	*Methylococcus*	Isolate	Patent RU2020129522A
GCF_026247885.1	Rice field soil; 10-15 cm deep	*Methylococcus*	Isolate	Awala SI et al (2023)
GCF_029478315.1	Mixture of strains (e.g., ATCC 33009; BKM 2116) from several laboratories followed by selection under specific conditions	*Methylococcus*	Isolate	Patent RU2613365C1
GCF_009498235.1	Acidic Sphagnum-dominated peat bog	*Methylospira*	Isolate	Danilova OV et al. (2016).
GCA_028688525.1	landfill. NEUS_C leachate from a leachate well at an active municipal landfill in the North Eastern United States	*Methylococcus*	MAG	Grégoire et al. (2023). M
GCA_003242955.1	Stratified humic lake	*Methyloumidiphilus*	MAG	Rissanen AJ, et al. (2018).
GCA_903912685.1	Lake sediment	*Methyloumidiphilus*	MAG	Buck M et al. (2021)
GCA_903831675.1	Lake sediment	*Methyloumidiphilus*	MAG	Buck M et al. (2021)
GCA_903831425.1	Lake sediment	*Methyloumidiphilus*	MAG	Buck M et al. (2021)
GCA_903929635.1	Lake sediment	*Methyloumidiphilus*	MAG	Buck M et al. (2021)
GCA_903882955.1	Lake water	*Methyloumidiphilus*	MAG	Buck M et al. (2021)
GCA_903848025.1	Lake water	*Methyloumidiphilus*	MAG	Buck M et al. (2021)
GCA_903896155.1	Lake water, Alinen Mustajärvi, 3m in depth	*Methyloumidiphilus*	MAG	Buck M et al. (2021)
GCA_903921065.1	Lake water, Alinen Mustajärvi, 4.4m in depth	*Methyloumidiphilus*	MAG	Buck M et al. (2021)
GCA_903908275.1	Lake water, Alinen Mustajärvi, 5.1m in depth	*Methyloumidiphilus*	MAG	Buck M et al. (2021)
GCA_903899245.1	Lake water, Alinen Mustajärvi, 5.8m in depth	*Methyloumidiphilus*	MAG	Buck M et al. (2021)
GCA_903834355.1	Lake water, Alinen Mustajärvi, 6.3 m in depth	*Methyloumidiphilus*	MAG	Buck M et al. (2021)
GCA_903877805.1	Lake water, Alinen Mustajärvi, 3m in depth	*Methyloumidiphilus*	MAG	Buck M et al. (2021)
GCA_903833575.1	Lake water, Alinen Mustajärvi, 4m in depth	*Methyloumidiphilus*	MAG	Buck M et al. (2021)
GCA_903835705.1	Lake water, Alinen Mustajärvi, 5.5m in depth	*Methyloumidiphilus*	MAG	Buck M et al. (2021)
GCA_903908235.1	Lake water, Alinen Mustajärvi, 6m in depth	*Methyloumidiphilus*	MAG	Buck M et al. (2021)
GCA_903911995.1	Lake water, Alinen Mustajärvi, 4m in depth	*Methyloumidiphilus*	MAG	Buck M et al. (2021)
GCA_903920655.1	Lake water, Alinen Mustajärvi, 4.5m in depth	*Methyloumidiphilus*	MAG	Buck M et al. (2021)
GCA_903823855.1	Lake water, Alinen Mustajärvi, 4.5 m deep	*Methyloumidiphilus*	MAG	Buck M et al. (2021)
GCA_903882195.1	Lake water, Alinen Mustajärvi, 5.5m in depth	*Methyloumidiphilus*	MAG	Buck M et al. (2021)
GCA_903898235.1	Lake water, Alinen Mustajärvi, 6m in depth	*Methyloumidiphilus*	MAG	Buck M et al. (2021)
GCA_903857375.1	Lake water, Alinen Mustajärvi, 3.5m in depth	*Methyloumidiphilus*	MAG	Buck M et al. (2021)
GCA_903835535.1	Lake water, Alinen Mustajärvi, 4m in depth	*Methyloumidiphilus*	MAG	Buck M et al. (2021)
GCA_903870715.1	Lake water, Alinen Mustajärvi, 4.5m in depth	*Methyloumidiphilus*	MAG	Buck M et al. (2021)
GCA_903901165.1	Lake water, Alinen Mustajärvi, 5m in depth	*Methyloumidiphilus*	MAG	Buck M et al. (2021)
GCA_903869035.1	Lake water, Alinen Mustajärvi, 5.5m in depth	*Methyloumidiphilus*	MAG	Buck M et al. (2021)
GCA_903879085.1	freshwater sediment, Alinen Mustajärvi	*Methyloumidiphilus*	MAG	Buck M et al. (2021)
GCA_903833305.1	freshwater sediment, Alinen Mustajärvi	*Methyloumidiphilus*	MAG	Buck M et al. (2021)
GCA_903878515.1	Lake water, 3.9m in depth	*Methyloumidiphilus*	MAG	Buck M et al. (2021)
GCA_903893045.1	Lake water, 4.2m in depth	*Methyloumidiphilus*	MAG	Buck M et al. (2021)
GCA_903882675.1	Lake water	*Methyloumidiphilus*	MAG	Buck M et al. (2021)
GCA_903881155.1	Lake water	*Methyloumidiphilus*	MAG	Buck M et al. (2021)
GCA_903906125.1	Lake water, 0.2 m in depth	*Methyloumidiphilus*	MAG	Buck M et al. (2021)

302 **Table 1**: List of genomes of *Methylococcales* containing *ccyA*. Main information about the genomes,
303 including whether they are derived from cultivated strain (isolate) or metagenomes (MAG), the genera
304 they are affiliated with, following GTDB classification, and their environmental origin. Additional
305 information is provided in Table S2.
306

307 **3.2 Comparison of *Cyanobacteria* and *Methylococcaceae* calcyanin sequences**

308 The calcyanin protein comprises two distinct domains: the N-terminal domain is short and
309 variable, and defines four calcyanin types in Cyanobacteria, called W (or CoBaHMA), X, Y
310 and Z, with the latter three restricted to specific clades (*Gloeomargarita, Fischerella* and
311 closely related genera, and *Microcystis*, respectively). In contrast, the C-terminal $(GlyZip)_3$
312 domain is much longer, characterized by a triplicated long glycine zipper, and it is highly
313 conserved across cyanobacteria. The conservation of this domain allows for the unambiguous
314 identification of calcyanin based solely on its sequence (Benzerara et al., 2022; Gaschignard et
315 al., 2024).

316 A multiple sequence alignment of the C-terminal domains revealed conservation of the
317 signature motifs of the $(GlyZip)_3$ domain in *Methylococcaceae* (Figure 2). Key features
318 included the repeated basic Gly-X(3)-Gly pattern within each GlyZip motif, interrupted at the
319 midpoint by a highly conserved Gly-Pro dipeptide. Additionally, several polar and aromatic
320 amino acids were notably conserved, particularly in the third GlyZip motif (indicated by stars
321 in Figure 2). Some variability was observed among *Methylococcaceae* members, principally
322 occurring outside the GlyZip motifs, similar to the variability observed across cyanobacteria.
323 Sequence comparisons further revealed that the *Methylococcaceae* C-terminal $(GlyZip)_3$
324 domains were more similar to Z-type calcyanins of *Microcystis* (47 % identity) than to other
325 calcyanin types found in other cyanobacteria (30 % identity). High and specific sequence
326 similarities were especially apparent in the first GlyZip motif of *Methylococcaceae* and
327 *Microcystis* (~60 % sequence identity versus lower than 40 % for other Cyanobacteria, Figure
328 2).

329 Additionally, the N-terminal domains of *Microcystis* Z-type calcyanins and *Methylococcaceae*
330 calcyanins also shared several features: they lacked strongly hydrophobic amino acids and were
331 enriched in alanine and polar residues (Figure S2). This property is also shared by the N-
332 terminal sequences of type-X and type-Y calcyanins. However, despite these compositional
333 similarities, no robust sequence alignments could be established between the *Microcystis* and
334 *Methylococcaceae* N-terminal sequences, as it was also the case between *Methylococcaceae*
335 and type X and type Y N-terminal sequences.-We note that similarly, no significant sequence
336 alignments could be established between the N-terminal sequences of the different
337 cyanobacterial calcyanins, the so-called CoBaHMA-, X-, Y- and Z-type calcyanins and yet they
338 are all markers of iACC biomineralization (Benzerara et al., 2022).
339 Three-dimensional (3D) structure predictions generated by AlphaFold3 suggested that the three
340 GlyZip motifs comprising the C-terminal domain of calcyanin share a common hairpin structure
341 (Figure 3). This structure consists of two tightly packed alpha-helices, whose close packing is
342 provided by glycine zippers (Figure 3). Even though the 3D structure of the GlyZip motifs are
343 predicted with low pLDDT values (<50), confidence can be placed in the models of the GlyZip
344 core region, spanning positions -4 to 4, over approximately 40 residues. This core region
345 exhibits structural similarity across the three GlyZip motifs within a single species and among
346 different species (see the RMSD values in Table S3). In contrast, structural variability is
347 observed in the AlphaFold3 models, even those built for a same sequence, particularly at the
348 N- and C-terminal extremities (thus outside the GlyZip core). The sole exception is GlyZip1,
349 for which the glycine zipper and associated helix packing invariably extends to these terminal
350 regions across all models (Figure 3). Consequently, only the entire GlyZip1 motif permits
351 structural comparisons between species, given the stability of its 3D structure predictions across
352 its full length. In contrast, the variability observed in models of a same sequence precludes any
353 meaningful comparison of the GlyZip2 and GlyZip3 motifs. These analyses revealed that the

3D structure of GlyZip1 in *Methylococcaceae* is structurally more similar to that of *Microcystis* than to those of other cyanobacteria (Figure 3 and metrics in Table S3). This similarity extends to the N-terminal domains, located upstream of the (GlyZip)3 domains, which are predicted to form alpha-helices structures, though with low confidence scores (Figure S2) and without any possibility to align the sequences. Importantly, AlphaFold3 failed to accurately predict the spatial arrangement between the three GlyZip motifs, indicating that the $(GlyZip)_3$ domain may adopt an as-yet-unknown 3D fold.

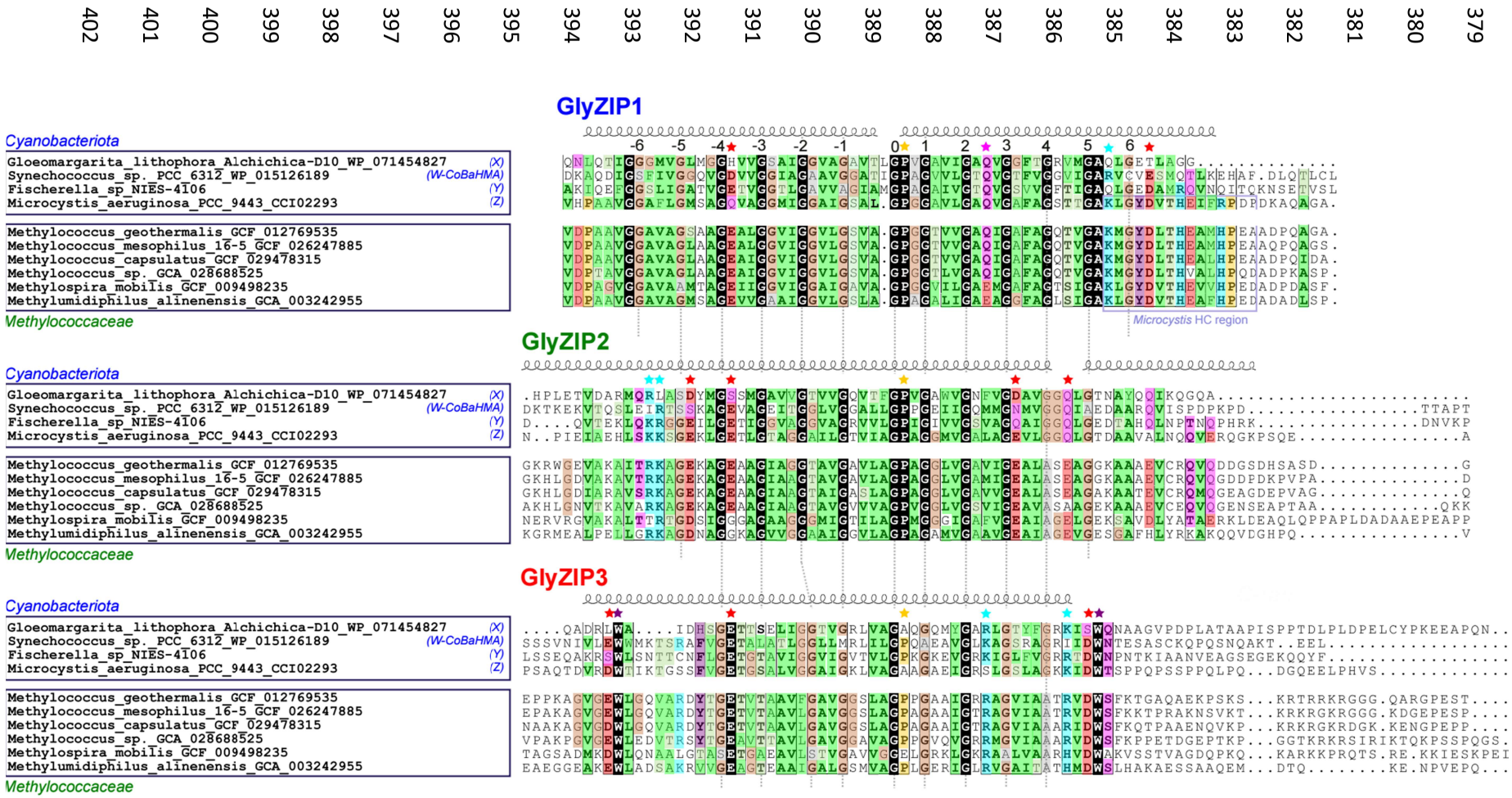

Figure 2: Comparison of the sequences of calcyanin GlyZip motifs of *Methylococcaceae* and cyanobacteria. Four calcyanin sequences representative of the different clades were selected for cyanobacteria, while for *Methylococcaceae,* six non-redundant ones were extracted from Table 1. The *Fischerella* sp. NIES-4106 calcyanin sequence was chosen as it has three GlyZip motifs, instead of two for most of the calcyanin sequences of this clade. Identities are shown in white on a black background, while similarities are highlighted with colors, according to amino acid properties and position in the alignment (with highly similar positions indicated in bold). The periodic motif involving glycine (or a small amino acid) every four residues is highlighted by numbers relative to the central conserved proline (gold star), and can be followed from one GlyZip motif to the next using vertical dotted lines. Highly conserved polar/aromatic positions are highlighted with stars. The lilac pink box highlights a region which is highly conserved (HC) between the *Microcystis* and *Methylococcaceae* sequences. The secondary structures (α-helices) as predicted by AlphaFold3 (pLDDT<70) on the *Methylococcus geothermalis* sequence are shown on top of the alignment.

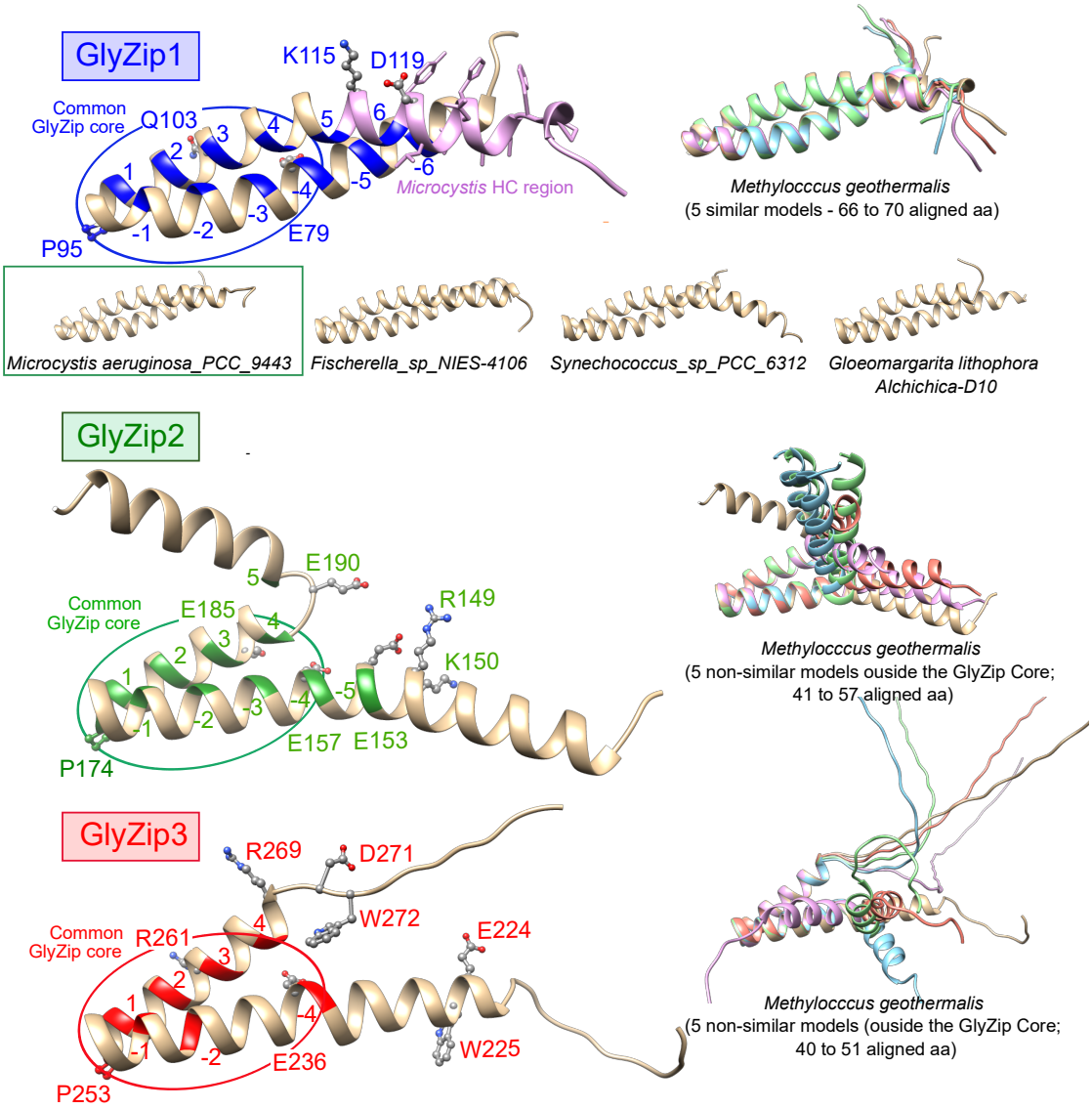

Figure 3: Ribbon representation of the 3D structure of the GlyZip motifs, as predicted by Alphafold3 using the *Methylococcus geothermalis* calcyanin sequence. The GlyZip motifs were superimposed for comparative analysis (metrics in Table S3). The periodic motifs involving glycine (or a small amino acid) every four residues are colored on the ribbons. Highly conserved charged/polar/aromatic residues (stars in Figure 2) are depicted in atomic details. The highly conserved (HC) region between the *Microcystis* and *Methylococcaceae* sequences (Figure 2) is highlighted in lilac pink. For note, the Alphafold3 per-residue pLDDT values are < 50, probably due to the fact that no template could be found in the Protein Data Bank to support the relevance of this prediction (and not because of a dubious prediction, a hypothesis ruled out by in-depth analysis of the model, in particular highlighting the common central GlyZip core around the Gly-Pro sequence). Structural uncertainties concern the N- and C-terminal extremities of the GlyZip motifs 2 and 3, which considerably vary (even in the five models built based on the same sequence from *Methylococcus geothermalis* – shown at right, mean RMSD and TM scores of 2.88 Å / 0.57 (41 to 57 aligned aa) for GlyZip2 and 2.57 Å / 0.43 (40 to 51 aligned aa) for GlyZip3), and which deviate from the packing imposed by the periodic repetitions of glycine. In contrast, GlyZip1 motif 3D structures are similar across the models of *M. geothermalis* calcyanin (1.57 Å / 0.86 (66 to 70 aligned aa)) and across the calcyanins of different species, as supported by RMSD values and TM-scores reported in Table S3. Overall, the GlyZip1 motifs and the GlyZip cores of GlyZip2 and GlyZip3 motifs in *Methylococcus geothermalis* exhibit greater structural similarity to those of *Microcystis aeruginosa* calcyanin than to calcyanins from other cyanobacteria.

423 Moreover, the similarity between the Z-type calcyanins of *Microcystis* and the newly identified
424 calcyanins of *Methylococcaceae* is strongly supported by phylogenetic analysis. Indeed, a
425 maximum likelihood tree constructed using the conserved GlyZip motifs in the C-terminal
426 domain of all calcyanins, showed that the *Microcystis* and *Methylococcaceae* sequences are
427 closely related with maximal statistical support (Figure 4). Interestingly, the phylogenetic
428 relationships among the *Methylococcaceae* GlyZip sequences perfectly mirrored those derived
429 from the phylogenomic analysis based on a large set of conserved markers from the
430 corresponding *Methylococcaceae* species (Figure 4). This mirroring indicates that the *ccyA*
431 gene has followed the speciation history of these species.

432
433

Figure 4: Maximum likelihood phylogenetic tree of the GlyZip domain of the calcyanin sequences. Calcyanin sequences of *Methylococcaceae* species are highlighted in green. The different types of cyanobacterial calcyanins (X, W/CoBaHMA, Y, and Z) are indicated. For the *Methylococcaceae*, a species tree based on the concatenation of 120 conserved markers is shown on the left (this tree is rooted on an outgroup composed of *Methylococcaceae* sp. GCA_902812445.1, *Methylotetracoccus* sp. GCA_025458755.1, *Methylotetracoccus* sp. GCA_004168015.1, and *Methylotetracoccus oryzae* GCF 006175985.1). Numbers on branches show ultrafast bootstrap values. The sequences used in the comparison of calcyanin sequences in Figure 2 appear in bold here.

447 **3.3 Experimental evidence of iACC formation by *Methylococcaceae* cultivated strains**

448 Both genomes of the cultivated strains *Methylococcus geothermalis* IM1 and *Methylococcus*
449 *mesophilus* 16-5 contain the *ccyA* gene (based on the signature of the C-terminal domain of
450 calcyanin), which is indicative of iACC formation in cyanobacteria. Consequently, we searched
451 for the presence of iACC in these strains. Laboratory cultures exhibited a typical exponential
452 growth curve, with a doubling time of 5.8±0.1 h for *M. geothermalis* and 13.1±0.8 h for *M.*
453 *mesophilus* (Figure S3).

454 Attenuated total reflectance Fourier transform infrared (ATR-FTIR) spectroscopy performed
455 on cell pellets showed unambiguously the presence of ACC in both *Methylococcaceae*
456 cultivated strains (Figure 5 and Table S4 for band assignment). Indeed, spectra showed a band
457 at around 860 cm^{-1}, detected in both *M. geothermalis*, *M. mesophilus*, a synthetic ACC reference
458 and iACC-forming cyanobacteria, but absent in a reference calcite and non-iACC-forming
459 cyanobacteria, and that was shown to be characteristic of ACC (Mehta et al., 2022b). Other
460 features observed in the spectra were bands at 1641 and 1528 cm^{-1}, identified as amide I and
461 amide II bands (Figure 5). Bands at 1444 and 1391 cm^{-1} detected in both *M. geothermalis* and
462 *M. mesophilus*, are similar to those observed at 1474 and 1395 cm^{-1} in ACC but they are not
463 exclusive to iACC-forming cyanobacteria and likely correspond to methyl groups in lipids
464 and/or C-O groups in carboxylic acids.

465 This finding was further corroborated by X-ray absorption near-edge structure (XANES)
466 spectroscopy at the Ca K-edge conducted on *M. geothermalis* cells. The derivative of the Ca K-
467 edge XANES spectrum of *M. geothermalis* cell pellets closely matched that of synthetic ACC
468 and iACC in cyanobacteria, distinguishing it from calcite and non-iACC-forming cyanobacteria
469 (Figure 6; Mehta et al., 2023). Specifically, the B1 feature in the derivative spectrum, which
470 was shifted compared to calcite, indicated the presence of ACC. Linear combination fitting
471 (LCF) of the XANES data revealed that approximately ~57% of the Ca in *M. geothermalis* was

in the form of ACC, with the remaining 43% of Ca likely complexed by organics and/or associated with polyphosphates (Figure 6).

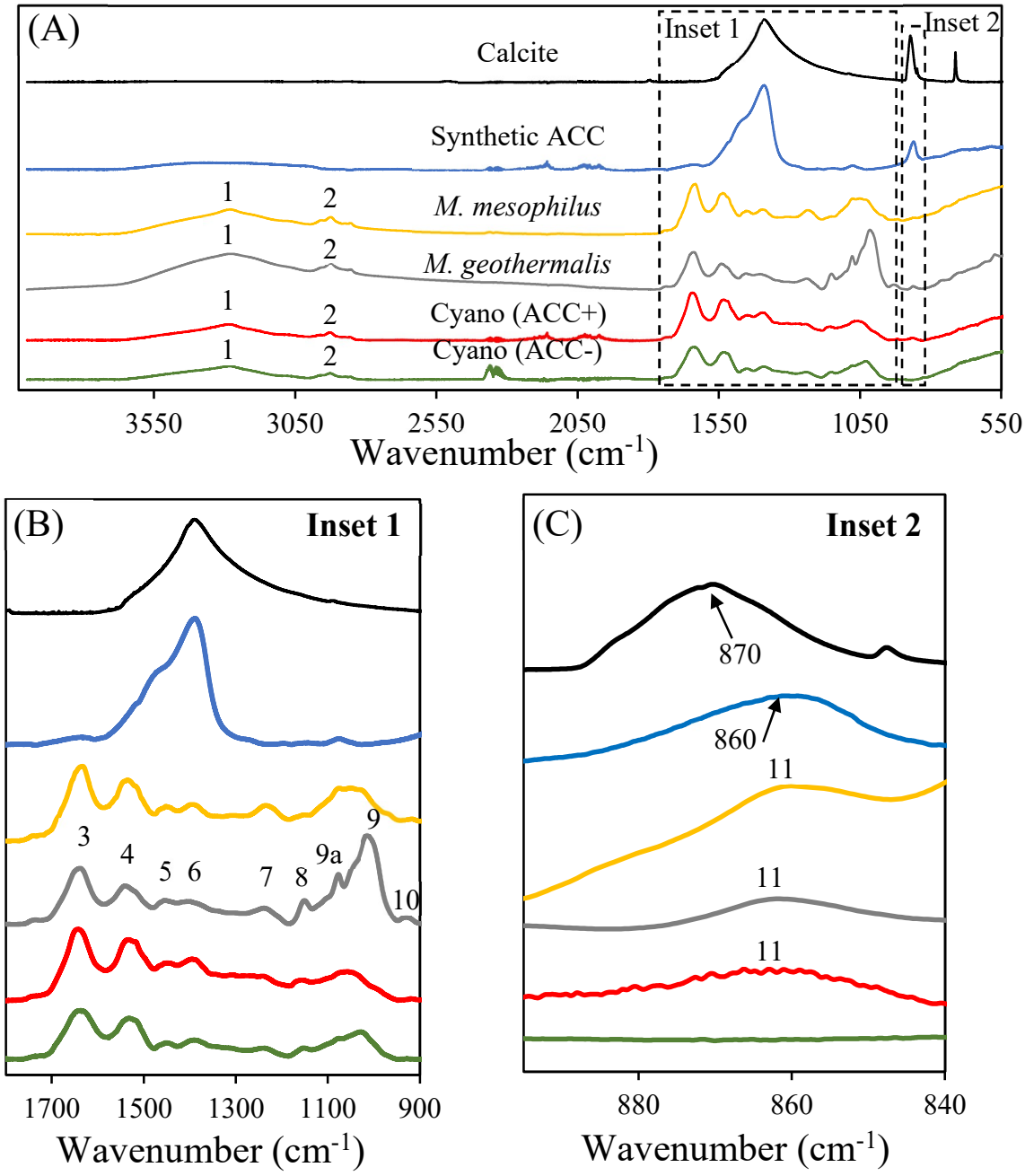

Figure 5: (A) ATR-FTIR spectra of *Methylococcus geothermalis* and *M. mesophilus* in the mid-IR range compared with reference spectra. Reference spectra are given for calcite, synthetic ACC, iACC-forming cyanobacteria (Cyano(ACC+)) and non-iACC-forming cyanobacteria (Cyano(ACC-)). The dashed rectangle envelops the zoomed regions of mid-IR ACC spectra shown in the inset 1 (1800–900 cm^{-1}) in (B), and inset 2 (950–820 cm^{-1}) in (C). Numbers on the spectra correspond to the band numbers and their assignments are provided in Table S4. Band 11 at 860 cm-1 is indicative of ACC.

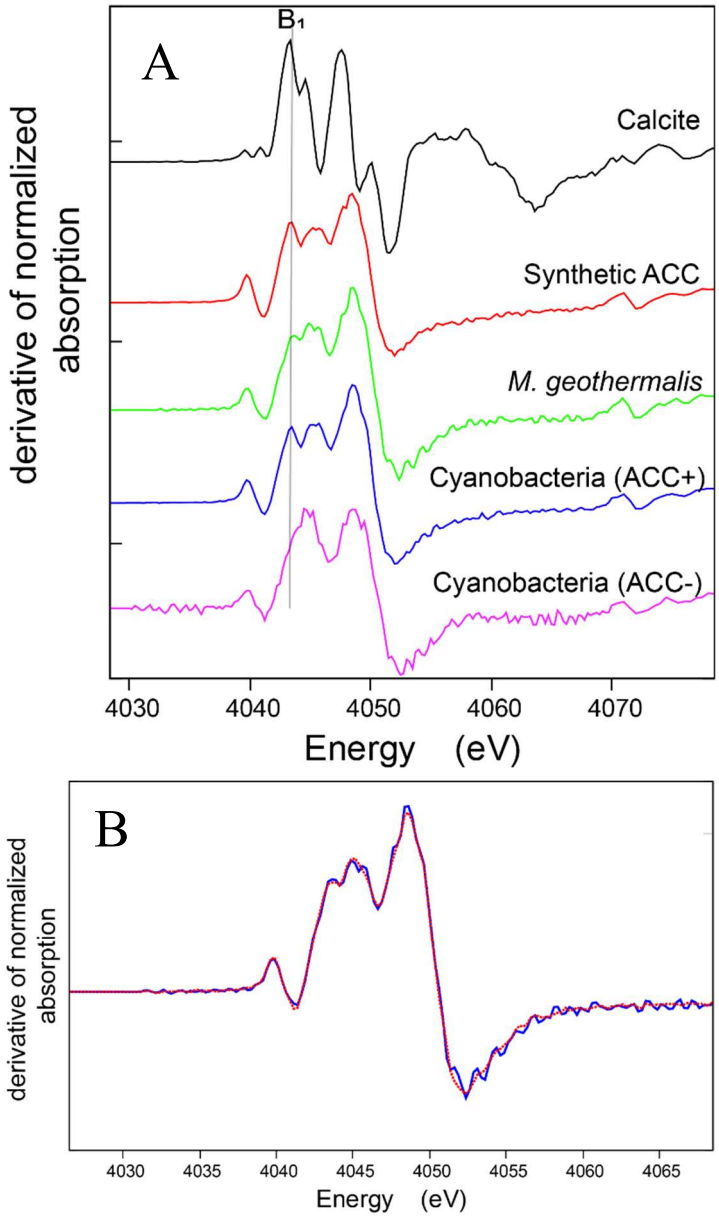

Figure 6: (A) Derivate XANES spectra at the Ca K-edge of *Methylococcus geothermalis* cell pellets compared with reference derivate spectra of calcite, synthetic ACC, iACC-forming cyanobacteria and non-iACC-forming cyanobacteria. The presence of a peak noted B1 indicated by a dashed line is indicative of ACC. (B) Linear combination fitting (LCF) of the derivate XANES spectrum of *Methylococcus geothermalis* cell pellets at the Ca K-edge. The solid line shows experimental data and the dotted line corresponds to the LCF result.

Consistently, both scanning electron microscopy (SEM) and scanning transmission electron microscopy (STEM) in the high-angle annular dark-field (HAADF) imaging mode combined with energy dispersive x-ray spectrometry (EDXS) showed that cells of both strains contained Ca-rich inclusions with some Mg but no S and no P, interpreted as calcium carbonate inclusions

(Figure 7 and Figure S4-6). Besides, cells also contained granules rich in phosphorus (P), with some Mg and K, interpreted as polyphosphate inclusions (Rivas-Lamelo et al., 2017).

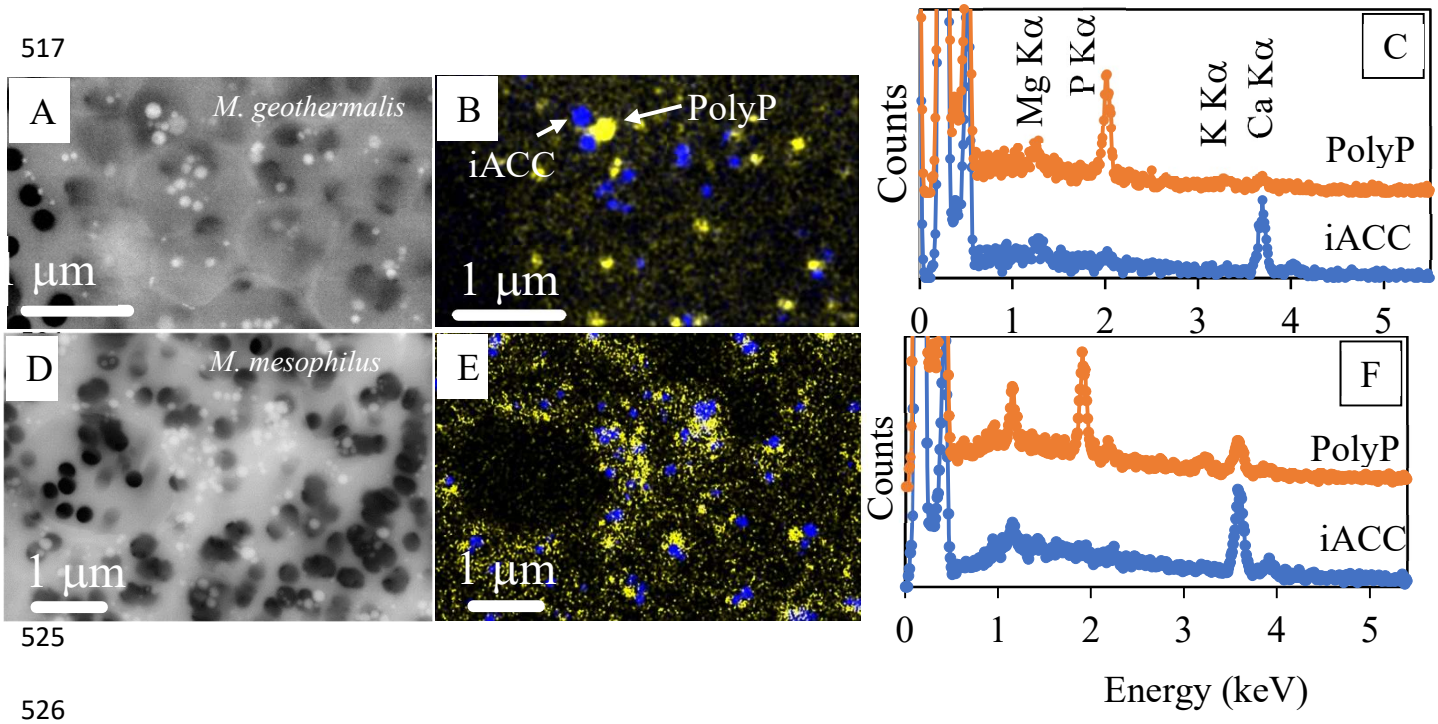

Figure 7: Scanning electron microscopy analyses of cultivated *Methylococcaceae*. (A-C) *Methylococcus geothermalis*. (A) Backscattered electron image. (B) Overlay of Ca (blue) and P (yellow) EDXS maps showing iACC and polyphosphate inclusions, respectively. (C) Characteristic EDXS spectra of polyphosphate (orange) and iACC (blue) inclusions. Emission lines of Mg Ka, P Ka, K Ka and Ca Ka are indicated. (D-F) Same analyses for *M. mesophilus*. More complete datasets can be viewed in the Supplementary Figures.

Last, cryo-soft X-ray tomography (c-SXT) was used to image vitrified *M. geothermalis* cells in a near-native state (15 cells in total, 6 cells used for volume reconstruction). Ca-rich inclusions were observed as regions of higher intensity (Figure 8A and Figure S7). These inclusions are most evident in the tomograms due to their strong absorption contrast and small, spherical morphology (Figure 8A). The absorption contrast from Ca-rich inclusions is much higher than other structures inside the cell (Figure 8B). Clearly defined Ca-rich inclusions were segmented to determine their average size and distribution, yielding a mean diameter of 118 ± 45 nm (n = 58) (Figure 8C). Other structural features, such as intracytoplasmic membranes and phosphate inclusions (Awala et al., 2020), can be distinguished from the smaller Ca-rich inclusions in the

tomograms but not from each other due to their similar linear absorption contrast coefficients (beige structures in Figure 8D). For whole-cell segmentation, these structures were therefore grouped as a single material. Figure 8D shows the 3D volume reconstruction of the two cells from Figure 8A, highlighting the outer cell membrane, intracytoplasmic membranes/phosphate inclusions, and Ca-rich inclusions. At least 10 Ca-rich inclusions were found per cell.

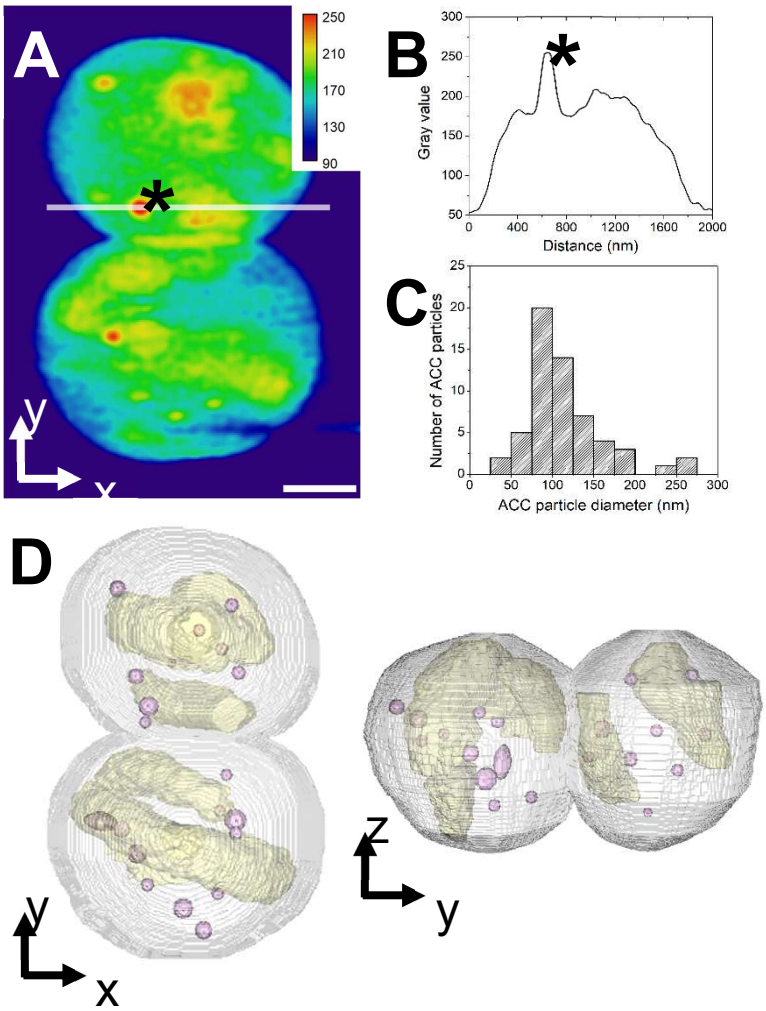

Figure 8: Cryo-soft X-ray tomography (c-SXT) of two ice-vitrified *Methylococcus geothermalis* cells. The image intensity corresponds to X-ray absorption by intracellular material at 520 eV—an energy within the "water window," where absorption by C and N atoms provides contrast of biological structures without chemical staining. At this energy, absorption by O atoms is minimal, allowing X-ray transmission through both the ice layer and hydrated cells. In contrast, the Ca $L_{2,3}$-edge at 350 eV enables detection of Ca atoms within the cells. (A) Virtual mid-cell z-slice of two *M. geothermalis* cells in reconstructed tomogram (an additional tomogram of two different cells is shown in Figure S3, along with tomogram videos for each dataset). Intensity scale (rainbow colour code) refers to absorption values. Asterisk marks the position of a Ca-rich inclusion. Scale bar is 500 nm. (B) Absorption profile extracted from horizontal line in (A) (asterisk marks the position of a Ca-rich inclusion). (C) Particle size distribution of Ca-rich granules measured from segmented volumes of the tomogram. (D) Volume

560 reconstruction of cells in (A) shown in two perspectives with Ca-rich granules in pink, intracytoplasmic
561 membranes/phosphate inclusions in beige and outer cell membrane in grey.
562

563 ## 3. Discussion

564 ### 4.1 Formation of iACC inclusions by bacteria remains an overlooked process

565 Here we report the discovery of iACC in members of the *Methylococcaceae*. This clade expands
566 the growing list of bacteria known to biomineralize ACC, which already includes *Achromatium*
567 (Benzerara et al., 2021; Gray, 2006; Schewiakoff, 1893), numerous phylogenetically diverse
568 members of the cyanobacteria (Benzerara et al., 2022), several magnetotactic *Pseudomonadota*,
569 spanning both *Gammaproteobacteria* and *Alphaproteobacteria*, and magnetotactic
570 *Nitrospirota* (Liu et al., 2021, 2025; Mangin et al., 2025; Monteil et al., 2020). Collectively,
571 these discoveries suggest that iACC biomineralization is more widespread than previously
572 recognized but has often gone unnoticed, likely due to the analytical challenges associated with
573 detecting ACC. Indeed, amorphous carbonates are highly labile and require dedicated
574 techniques for reliable identification (Addadi et al., 2003).
575 For example, although the ultrastructures of *M. geothermalis* and *M. mesophilus* had previously
576 been examined using electron microscopy, iACC granules were not reported (Awala et al.,
577 2020, 2023). This omission can be explained both by the distinct objectives of those studies
578 that did not target mineralogy and the absence of chemical analyses suited to the detection of
579 iACC. In contrast, our combined use of STEM-EDXS on intact, untreated cells together with
580 Ca K-edge XANES and/or FTIR spectroscopy enabled the unambiguous detection of iACC in
581 both species. Moreover, iACC granules were likely lost during the ultramicrotomy preparations
582 employed by Awala et al. (2020 & 2023) since standard protocols involving chemical fixation,
583 post-fixation and dehydration are known to dissolve iACC in cyanobacteria (Blondeau et al.,
584 2018a; Li et al., 2016). It is therefore possible that the numerous electron-translucent vesicles
585 or intracellular inclusions previously interpreted as polyphosphate or glycogen granules by
586 Awala et al. (2020, 2023) actually represent dissolved or transformed iACC granules. However,

587 this hypothesis can only be rigorously tested using cryo-electron microscopy of vitreous
588 sections (CEMOVIS).
589 An additional and pivotal line of evidence for iACC biomineralization in the *Methylococcaceae*
590 was the detection of the *ccyA* gene (and more specifically the portion encoding the characteristic
591 C-terminal $(GlyZip)_3$ domain of calcyanin), previously identified as a diagnostic marker of
592 iACC formation in cyanobacteria (Benzerara et al., 2022). Our findings extend the diagnostic
593 value of *ccyA* beyond cyanobacteria, although so far, no other clades represented in current
594 genomic databases appear to carry this gene—unless their versions of *ccyA* have diverged
595 substantially. Importantly, however, the absence of *ccyA* in other bacterial lineages does not
596 necessarily imply the absence of iACC formation. For instance, some magnetotactic
597 *Pseudomonadota* and *Achromatium* both form iACC despite lacking *ccyA*, suggesting that
598 multiple, distinct molecular pathways may give rise to iACC biomineralization (Mangin et al.,
599 2025).
600 Last, numerous MAGs of iACC-forming *Methylococcaceae* that we have detected originate
601 from chemically stratified boreal lakes and ponds (Table 1; Buck et al., 2021). Interestingly,
602 MAGs from other bacteria phylogenetically close to iACC-forming magnetotactic bacteria
603 were also found in the same stratified lakes and ponds in Finland and Sweden (Mangin et al.,
604 2025), suggesting that iACC biomineralization might be a geochemically important process in
605 these lakes.
606
607 **4.2 Relationship between *Methylococcaceae* metabolism and iACC biomineralization**
608 The mechanisms governing iACC biomineralization remain poorly understood. It has been
609 proposed that bacterial primary metabolism may play an important role in driving this process
610 (Görgen et al., 2020). In *Achromatium*, a sulfur-oxidizing bacterium, iACC formation is linked
611 to sulfide oxidation to elemental sulfur (Yang et al., 2019). This reaction consumes protons,

612 thereby increasing intracellular pH. The resulting shift in carbonate equilibrium favors the
613 conversion of bicarbonate (HCO_3^-) to carbonate ions (CO_3^{2-}), which in turn promotes calcium
614 carbonate precipitation. Conversely, when elemental sulfur is oxidized to sulfate, protons are
615 released, decreasing intracellular pH and causing iACC dissolution. Thus, iACC function as a
616 dynamic pH buffer: consuming protons through their dissolution and releasing them through
617 their precipitation.
618 A similar hypothesis has been proposed for cyanobacteria, where photosynthesis elevates
619 intracellular pH and thereby increases carbonate ion concentration, favoring iACC precipitation
620 (Li et al., 2016). While these models hold for *Achromatium* and cyanobacteria, the present study
621 shows that a proton-consuming primary metabolism is not strictly required for iACC
622 biomineralization. In *Methylococcaceae*, aerobic methanotrophy does not consume protons, as
623 shown by equation (1):
624 $CH_4 + 2O_2 = CO_2 + 2H_2O$ (1)
625 Moreover, the CO_2 produced by aerobic methanotrophs should promote calcium carbonate
626 dissolution as shown by Krause et al. (2014) and according to carbonate equilibria:
627 $CaCO_3 + CO_2 + H_2O = Ca^{2+} + 2HCO_3^-$ (2)
628 However, a portion of this CO_2 may be diverted into small organic molecules via RuBiSCO-
629 mediated carbon fixation, as shown in *Methylococcus*, and may therefore not react with $CaCO_3$
630 (Oshkin et al., 2021). Overall, iACC precipitation in *Methylococcaceae* likely relies on an
631 additional, secondary metabolic process—yet to be identified—that consumes protons and
632 converts CO_2 into carbonate ions so that:
633 $CO_2 + H_2O = H_2CO_3$
634 $H_2CO_3 + Ca^{2+} + 2OH^- = CaCO_3 + 2H_2O$
635 Alternatively, if CO_2 fixation exceeds CO_2 release from methanotrophy, the net CO_2 production
636 by the cell would become at least sometimes negative, shifting the carbonate equilibrium

637 towards carbonate ions and favoring iACC precipitation. This hypothesis aligns with recent
638 findings in magnetotactic iACC-forming *Alphaproteobacteria*, whose primary metabolism
639 does not induce alkalinization but appears to support CO_2 fixation (Mangin et al., 2025).
640 Finally, calcium uptake is essential for storage within iACC. Ca^{2+}/H^{+} protein exchangers (Cax
641 proteins) are plausible candidates and we have detected *cax* genes in *Methylococcaceae*
642 genomes (data not shown). However, these transporters are generally inferred to function in
643 calcium efflux rather than uptake in bacteria (Waditee et al., 2004), which contradicts the
644 requirements for iACC formation. Future studies are needed to elucidate the specific metabolic
645 and transport processes enabling iACC biomineralization in *Methylococcaceae*. Aerobic
646 methane-oxidizing bacteria are widespread in many aquatic systems and have a significant
647 environmental and ecological role since they are key in the regulation of emissions of CH_4, a
648 potent greenhouse gas, and provide CH_4-derived organic carbon compounds to surrounding
649 heterotrophic microorganisms (Khanongnuch et al., 2022). How the capability to biomineralize
650 iACC in some of these organisms may play an overlooked regulatory role in these important
651 biogeochemical processes remains to be understood.
652
653 **4.3 Evolutionary origin of iACC biomineralization in *Methylococcaceae***
654 The *ccyA* gene has an ancient origin within cyanobacteria, explaining its broad phylogenetic
655 distribution across the phylum, with multiple secondary losses in modern lineages (Benzerara
656 et al., 2022). As mentioned above, *ccyA* genes encode calcyanin proteins composed of a long,
657 conserved C-terminal $(GlyZip)_3$ domain and a short N-terminal domain, which exhibits
658 variability across species. This difference between the two domains suggests that there is a
659 strong selective pressure acting on the C-terminal domain, keeping it largely invariant, whereas
660 the N-terminal domain appears much less constrained and free to vary. These contrasting
661 evolutionary pressures have driven the diversification of several calcyanin families in
662 cyanobacteria, each characterized by distinct N-terminal domains, termed CoBaHMA, X, Y,

663 and Z. The X, Y, and Z types are restricted to specific clades, i.e., *Gloeomargarita*, *Fischerella*
664 (and closely related genera), and *Microcystis*, respectively. In contrast, the CoBaHMA-type
665 calcyanin occurs in several distantly related lineages and has therefore been proposed as the
666 most ancient form of calcyanin (Benzerara et al., 2022).
667 The calcyanin sequences identified in *Methylococcaceae* have specific characteristics not found
668 in the four cyanobacterial types but share clear sequence and structural similarities with the
669 *Microcystis* (Z-type) calcyanins, which can be observed especially over the GlyZip1 motif of
670 the (GlyZip)3 domain but also in the N-terminal domain. This is unexpected given the vast
671 evolutionary distance between *Methylococcaceae* and all the cyanobacterial clades.
672 Phylogenetic analysis strongly supports the relationship between the *Methylococcaceae* and
673 cyanobacterial sequences (Figure 4). The most parsimonious explanation for this observation
674 is that *Methylococcaceae* acquired *ccyA* through horizontal gene transfer (HGT) from a
675 cyanobacterial ancestor closely related to *Microcystis*. Alternative explanations would be that
676 (i) *ccyA* was present in the last common ancestor of *Methylococcaceae* and *Cyanobacteria*—
677 two highly distant lineages—and subsequently lost independently thousands of times in all
678 other bacterial lineages, or (ii) that *Methylococcaceae* and *Cyanobacteria* independently
679 evolved (GlyZip)3-encoding genes with similar amino acid residues at key positions and
680 independently linked them to small, variable N-terminal domains. However, both scenarios are
681 far less parsimonious than the hypothesis of a single HGT event between *Methylococcaceae*
682 and *Cyanobacteria*. The fact that the phylogeny of the *Methylococcaceae* calcyanin sequences
683 mirrors that of the corresponding species (Figure 4), strongly suggests a single HGT acquisition
684 by an ancient *Methylococcaceae* species, followed by subsequent divergence in several
685 *Methylococcaceae* subgroups, including several independent losses in the contemporary
686 *Methylococcaceae* lineages lacking *ccyA*. Such independent losses have also been proposed to

687 explain the current distribution of *ccyA* in the contemporary cyanobacterial lineages (Benzerara
688 et al., 2022).
689 About 1/3 of known *Microcystis* genomes contain *ccyA*, which was also likely ancestral in this
690 genus and lost secondarily in several lineages (Gaetan et al., 2023). Consistently with the
691 presence of *ccyA*, abundant iACC-forming *Microcystis* strains have been observed in several
692 lakes (Gaetan et al., 2023). One plausible ecological setting for the HGT of *ccyA* from
693 *Microcystis* to *Methylococacceae* is exemplified by Lake Cadagno, a meromictic lake (i.e.,
694 permanently stratified with an anoxic monimolimnion). At its chemocline, methane removal is
695 driven by aerobic methane oxidizers which are physically associated with cyanobacteria
696 (Milucka et al., 2015). More precisely, physical associations between *Microcystis* and diverse
697 *Methylococcales* are common in lakes and ponds, where they may be responsible for an
698 overlooked sink for methane (Li et al., 2021). Similarly, microbial consortia comprising
699 cyanobacteria and methanotrophic bacteria are employed in oxygen-deficient wastewater
700 treatment plants to remove methane (Safitri et al., 2021). In these consortia, cyanobacteria
701 produce O_2 that fuels aerobic methanotrophy, while the resulting CO_2 is taken up by the
702 phototrophs. Such tight metabolic coupling provides an ideal setting for close and sustained
703 interactions between cyanobacteria and *Methylococcales*, potentially facilitating HGT. One of
704 these HGT events appears to have transmitted the capability to biomineralize iACC from
705 cyanobacteria to *Methylococcaceae*.
706
707 **Conclusions**
708 This study shows that aerobic methanotrophs belonging to the *Methylococcaceae* family form
709 iACC. They most likely acquired the *ccyA* gene, a diagnostic marker of iACC biomineralization
710 in cyanobacteria, through HGT from an ancestral *Microcystis*-like cyanobacterial donor. This
711 HGT event may have taken place in a permanently stratified lake or in any other anoxic-oxic
712 transition zone in aquatic habitats, where *Microcystis* and *Methylococcaceae* can co-exist.

713 *Methylococcaceae* forming iACC may be abundant in some environments. Yet, how iACC are
714 formed and, in particular, how much of the carbon from methane oxidation is stored within
715 iACC and diverted from the production of small organic carbon molecules by these bacteria
716 remains to be quantified.
717

718 **Data Availability Statement**

719 All gene sequences were retrieved from GTDB as indicated in the Material and Method section
720 and no new sequence was generated by this study. Microscopy and spectroscopy data are
721 available on Zenodo: https://doi.org/10.5281/zenodo.17846939
722

723 **Acknowledgements**

724 This study was supported by the Agence Nationale de la Recherche (ANR), under grants
725 Cyanoman, ANR-24-CE44-5543 and Carbomagnet ANR-21-CE01-0010 and the ERC grants
726 Calcyan (PI: K. Benzerara, Grant Agreement no. 307110) and Plast-Evol (PI: D. Moreira, Grant
727 Agreement no. 787904. We thank synchrotron ALBA (Barcelona, Spain) for providing
728 beamtime on the cryo transmission X-ray microscopy at the Mistral beamline under proposal
729 number 2023027368. We thank synchrotron SOLEIL (Saclay, France) for providing beamtime
730 to conduct XANES measurements on the LUCIA beamline under proposal number 20220623.
731 We also thank the IMPMC analytical platforms that enabled the data acquisition: Imène Estève
732 for the SEM-EDXS support; Maxime Guillaumet and Keevin Beneut for IR spectroscopy
733 support at IMPMC.
734

735 **Conflict of interest statement**

736 The authors declare no conflicts of interest.
737

738 **References**

Abramson, J., Adler, J., Dunger, J., Evans, R., Green, T., Pritzel, A., Ronneberger, O., Willmore, L., Ballard, A. J., Bambrick, J., Bodenstein, S. W., Evans, D. A., Hung, C.-C., O'Neill, M., Reiman, D., Tunyasuvunakool, K., Wu, Z., Žemgulytė, A., Arvaniti, E., Beattie, C., Bertolli, O., Bridgland, A., Cherepanov, A., Congreve, M., Cowen-Rivers, A. I., Cowie, A., Figurnov, M., Fuchs, F. B., Gladman, H., Jain, R., Khan, Y. A., Low, C. M. R., Perlin, K., Potapenko, A., Savy, P., Singh, S., Stecula, A., Thillaisundaram, A., Tong, C., Yakneen, S., Zhong, E. D., Zielinski, M., Žídek, A., Bapst, V., Kohli, P., Jaderberg, M., Hassabis, D., and Jumper, J. M.: Accurate structure prediction of biomolecular interactions with AlphaFold 3, Nature, 630, 493–500, https://doi.org/10.1038/s41586-024-07487-w, 2024.

Addadi, L., Raz, S., and Weiner, S.: Taking advantage of disorder: amorphous calcium carbonate and its roles in biomineralization, Advanced Materials, 15, 959–970, https://doi.org/10.1002/adma.200300381, 2003.

Awala, S. I., Bellosillo, L. A., Gwak, J.-H., Nguyen, N.-L., Kim, S.-J., Lee, B.-H., and Rhee, S.-K.: *Methylococcus geothermalis* sp. nov., a methanotroph isolated from a geothermal field in the Republic of Korea, International Journal of Systematic and Evolutionary Microbiology, 70, 5520–5530, https://doi.org/10.1099/ijsem.0.004442, 2020.

Awala, S. I., Kim, Y., Gwak, J.-H., Seo, C., Lee, S., Kang, M., and Rhee, S.-K.: *Methylococcus mesophilus* sp. nov., the first non-thermotolerant methanotroph of the genus *Methylococcus*, from a rice field, International Journal of Systematic and Evolutionary Microbiology, 73, 006077, https://doi.org/10.1099/ijsem.0.006077, 2023.

Bacchetta, T., López-García, P., Gutiérrez-Preciado, A., Mehta, N., Skouri-Panet, F., Benzerara, K., Ciobanu, M., Yubuki, N., Tavera, R., and Moreira, D.: Description of Gloeomargarita ahousahtiae sp. nov. (Gloeomargaritales), a thermophilic cyanobacterium with intracellular carbonate inclusions, European Journal of Phycology, 59, 11–20, https://doi.org/10.1080/09670262.2023.2216257, 2024.

Belevich, I., Joensuu, M., Kumar, D., Vihinen, H., and Jokitalo, E.: Microscopy Image Browser: A platform for segmentation and analysis of multidimensional datasets, PLOS Biology, 14, e1002340, https://doi.org/10.1371/journal.pbio.1002340, 2016.

Benzerara, K., Skouri-Panet, F., Li, J., Férard, C., Gugger, M., Laurent, T., Couradeau, E., Ragon, M., Cosmidis, J., Menguy, N., Margaret-Oliver, I., Tavera, R., López-García, P., and Moreira, D.: Intracellular Ca-carbonate biomineralization is widespread in cyanobacteria, PNAS, 111, 10933–10938, https://doi.org/10.1073/pnas.1403510111, 2014.

Benzerara, K., Bolzoni, R., Monteil, C., Beyssac, O., Forni, O., Alonso, B., Asta, M. P., and Lefevre, C.: The gammaproteobacterium *Achromatium* forms intracellular amorphous calcium carbonate and not (crystalline) calcite, Geobiology, 19, 199–213, https://doi.org/10.1111/gbi.12424, 2021.

Benzerara, K., Duprat, E., Bitard-Feildel, T., Caumes, G., Cassier-Chauvat, C., Chauvat, F., Dezi, M., Diop, S. I., Gaschignard, G., Görgen, S., Gugger, M., López-García, P., Millet, M., Skouri-Panet, F., Moreira, D., and Callebaut, I.: A new gene family diagnostic for intracellular biomineralization of amorphous Ca carbonates by cyanobacteria, Genome Biology and Evolution, 14, evac026, https://doi.org/10.1093/gbe/evac026, 2022.

Benzerara, K., Görgen, S., Athar, K. M., Chauvat, F., March, K., Menguy, N., Mehta, N., Skouri-Panet, F., Swaraj, S., Travert, C., Cassier-Chauvat, C., and Duprat, E.: Quantitative mapping of calcium cell reservoirs in cyanobacteria at the submicrometer scale, Journal of Electron Spectroscopy and Related Phenomena, 267, 147369, https://doi.org/10.1016/j.elspec.2023.147369, 2023.

Bitard-Feildel, T., Lamiable, A., Mornon, J.-P., and Callebaut, I.: Order in disorder as observed by the "Hydrophobic Cluster Analysis" of protein sequences, Proteomics, 18, e1800054, https://doi.org/10.1002/pmic.201800054, 2018.

Bittrich, S., Segura, J., Duarte, J. M., Burley, S. K., and Rose, Y.: RCSB protein Data Bank: exploring protein 3D similarities via comprehensive structural alignments, Bioinformatics, 40, btae370, https://doi.org/10.1093/bioinformatics/btae370, 2024.

Blondeau, M., Sachse, M., Boulogne, C., Gillet, C., Guigner, J.-M., Skouri-Panet, F., Poinsot, M., Ferard, C., Miot, J., and Benzerara, K.: Amorphous calcium carbonate granules form within an intracellular compartment in calcifying cyanobacteria, Front. Microbiol., 9, 1768, https://doi.org/10.3389/fmicb.2018.01768, 2018a.

Blondeau, M., Benzerara, K., Ferard, C., Guigner, J.-M., Poinsot, M., Coutaud, M., Tharaud, M., Cordier, L., and Skouri-Panet, F.: Impact of the cyanobacterium *Gloeomargarita lithophora* on the geochemical cycles of Sr and Ba, Chemical Geology, 483, 88–97, https://doi.org/10.1016/j.chemgeo.2018.02.029, 2018b.

Bruley, A., Gaëtan, J., Gugger, M., Pancrace, C., Millet, M., Gaschignard, G., Dezi, M., Humbert, J.-F., Leloup, J., Skouri-Panet, F., Callebaut, I., Benzerara, K., and Duprat, E.: Diel changes in the expression of a marker gene and candidate genes for intracellular amorphous $CaCO_3$ biomineralization in *Microcystis*, Peer Community Journal, 5, https://doi.org/10.24072/pcjournal.516, 2025.

Buck, M., Garcia, S. L., Fernandez, L., Martin, G., Martinez-Rodriguez, G. A., Saarenheimo, J., Zopfi, J., Bertilsson, S., and Peura, S.: Comprehensive dataset of shotgun metagenomes from oxygen stratified freshwater lakes and ponds, Sci Data, 8, 131, https://doi.org/10.1038/s41597-021-00910-1, 2021.

Cam, N., Benzerara, K., Georgelin, T., Jaber, M., Lambert, J.-F., Poinsot, M., Skouri-Panet, F., Moreira, D., Lopez-Garcia, P., Raimbault, E., Cordier, L., and Jézéquel, D.: Cyanobacterial formation of intracellular Ca-carbonates in undersaturated solutions, Geobiology, 16, 49–61, https://doi.org/10.1111/gbi.12261, 2017.

Capella-Gutiérrez, S., Silla-Martínez, J. M., and Gabaldón, T.: trimAl: a tool for automated alignment trimming in large-scale phylogenetic analyses, Bioinformatics, 25, 1972–1973, https://doi.org/10.1093/bioinformatics/btp348, 2009.

Chaumeil, P.-A., Mussig, A. J., Hugenholtz, P., and Parks, D. H.: GTDB-Tk v2: memory friendly classification with the genome taxonomy database, Bioinformatics, 38, 5315–5316, https://doi.org/10.1093/bioinformatics/btac672, 2022.

Cosmidis, J. and Benzerara, K.: Why do microbes make minerals?, Comptes Rendus. Géoscience, 354, 1–39, https://doi.org/10.5802/crgeos.107, 2022.

Couradeau, E., Benzerara, K., Gerard, E., Moreira, D., Bernard, S., Brown, G. E., and Lopez-Garcia, P.: An early-branching microbialite cyanobacterium forms intracellular carbonates, Science, 336, 459–462, https://doi.org/10.1126/science.1216171, 2012.

Flank, A.-M., Cauchon, G., Lagarde, P., Bac, S., Janousch, M., Wetter, R., Dubuisson, J.-M., Idir, M., Langlois, F., Moreno, T., and Vantelon, D.: LUCIA, a microfocus soft XAS beamline, Nuclear Instruments and Methods in Physics Research Section B: Beam Interactions with Materials and Atoms, 246, 269–274, https://doi.org/10.1016/j.nimb.2005.12.007, 2006.

822 Gaetan, J., Halary, S., Millet, M., Bernard, C., Duval, C., Hamlaoui, S., Hecquet, A., Gugger, M., Marie,
823 B., Mehta, N., Moreira, D., Skouri-Panet, F., Travert, C., Duprat, E., Leloup, J., and Benzerara, K.:
824 Widespread formation of intracellular calcium carbonates by the bloom-forming cyanobacterium
825 *Microcystis*, Environmental Microbiology, 25, 751–765, https://doi.org/10.1111/1462-2920.16322,
826 2023.

827 Gaschignard, G., Millet, M., Bruley, A., Benzerara, K., Dezi, M., Skouri-Panet, F., Duprat, E., and
828 Callebaut, I.: AlphaFold2-guided description of CoBaHMA, a novel family of bacterial domains within
829 the heavy-metal-associated superfamily, Proteins: Structure, Function, and Bioinformatics, 92, 776–
830 794, https://doi.org/10.1002/prot.26668, 2024.

831 Gilbert, P. U. P. A., Bergmann, K. D., Boekelheide, N., Tambutté, S., Mass, T., Marin, F., Adkins, J. F.,
832 Erez, J., Gilbert, B., Knutson, V., Cantine, M., Hernández, J. O., and Knoll, A. H.: Biomineralization:
833 Integrating mechanism and evolutionary history, Science Advances, 8, eabl9653,
834 https://doi.org/10.1126/sciadv.abl9653, 2022.

835 Görgen, S., Benzerara, K., Skouri-Panet, F., Gugger, M., Chauvat, F., and Cassier-Chauvat, C.: The
836 diversity of molecular mechanisms of carbonate biomineralization by bacteria, Discov Mater, 1, 2,
837 https://doi.org/10.1007/s43939-020-00001-9, 2020.

838 Gouet, P., Robert, X., and Courcelle, E.: ESPript/ENDscript: extracting and rendering sequence and 3D
839 information from atomic structures of proteins, Nucleic Acids Res, 31, 3320–3323,
840 https://doi.org/10.1093/nar/gkg556, 2003.

841 Gray, N. D.: The unique role of intracellular calcification in the genus *Achromatium*, in: Inclusions in
842 Prokaryotes, edited by: Shively, J. M., Springer, Berlin, Heidelberg, 299–309,
843 https://doi.org/10.1007/3-540-33774-1_11, 2006.

844 Hoang, D. T., Chernomor, O., von Haeseler, A., Minh, B. Q., and Vinh, L. S.: UFBoot2: Improving the
845 Ultrafast Bootstrap Approximation, Mol Biol Evol, 35, 518–522,
846 https://doi.org/10.1093/molbev/msx281, 2018.

847 Hyatt, D., Chen, G.-L., LoCascio, P. F., Land, M. L., Larimer, F. W., and Hauser, L. J.: Prodigal: prokaryotic
848 gene recognition and translation initiation site identification, BMC Bioinformatics, 11, 119,
849 https://doi.org/10.1186/1471-2105-11-119, 2010.

850 Katoh, K., Rozewicki, J., and Yamada, K. D.: MAFFT online service: multiple sequence alignment,
851 interactive sequence choice and visualization, Brief Bioinform, 20, 1160–1166,
852 https://doi.org/10.1093/bib/bbx108, 2019.

853 Khanongnuch, R., Mangayil, R., Svenning, M. M., and Rissanen, A. J.: Characterization and genome
854 analysis of a psychrophilic methanotroph representing a ubiquitous *Methylobacter* spp. cluster in
855 boreal lake ecosystems, ISME COMMUN., 2, 85, https://doi.org/10.1038/s43705-022-00172-x, 2022.

856 Larralde, M. and Zeller, G.: PyHMMER: a Python library binding to HMMER for efficient sequence
857 analysis, Bioinformatics, 39, btad214, https://doi.org/10.1093/bioinformatics/btad214, 2023.

858 Le, S. Q. and Gascuel, O.: An improved general amino acid replacement matrix, Mol Biol Evol, 25, 1307–
859 1320, https://doi.org/10.1093/molbev/msn067, 2008.

860 Li, C., Hambright, K. D., Bowen, H. G., Trammell, M. A., Grossart, H.-P., Burford, M. A., Hamilton, D. P.,
861 Jiang, H., Latour, D., Meyer, E. I., Padisák, J., Zamor, R. M., and Krumholz, L. R.: Global co-occurrence

of methanogenic archaea and methanotrophic bacteria in *Microcystis* aggregates, Environmental Microbiology, 23, 6503–6519, https://doi.org/10.1111/1462-2920.15691, 2021.

Li, J., Margaret Oliver, I., Cam, N., Boudier, T., Blondeau, M., Leroy, E., Cosmidis, J., Skouri-Panet, F., Guigner, J.-M., Férard, C., Poinsot, M., Moreira, D., Lopez-Garcia, P., Cassier-Chauvat, C., Chauvat, F., and Benzerara, K.: Biomineralization patterns of intracellular carbonatogenesis in cyanobacteria: molecular hypotheses, Minerals, 6, 10, https://doi.org/10.3390/min6010010, 2016.

Liu, P., Liu, Y., Ren, X., Zhang, Z., Zhao, X., Roberts, A. P., Pan, Y., Li, J., and Semrau, J. D.: A novel magnetotactic Alphaproteobacterium producing intracellular magnetite and calcium-bearing minerals, Applied and Environmental Microbiology, 87, e01556-21, https://doi.org/10.1128/AEM.01556-21, 2021.

Liu, P., Zhang, R., Meng, F., Zhang, C., Roberts, A. P., Wang, Y., Zhu, K., Cao, Z., Pan, Y., and Li, J.: Deep-branching magnetotactic bacteria form intracellular carbonates enriched in trace metals, mSystems, 0, e01131-25, https://doi.org/10.1128/msystems.01131-25, 2025.

Mangin, C. C., Benzerara, K., Bergot, M., Menguy, N., Alonso, B., Fouteau, S., Méheust, R., Chevrier, D. M., Godon, C., Turrini, E., Mehta, N., Duverger, A., Travert, C., Busigny, V., Duprat, E., Bolzoni, R., Cruaud, C., Viollier, E., Jézéquel, D., Vallenet, D., Lefèvre, C. T., and Monteil, C. L.: Magnetotactic bacteria affiliated with diverse *Pseudomonadota* families biomineralize intracellular Ca-carbonate, The ISME Journal, 19, wrae260, https://doi.org/10.1093/ismejo/wrae260, 2025.

Mehta, N., Benzerara, K., Kocar, B. D., and Chapon, V.: Sequestration of radionuclides Radium-226 and Strontium-90 by cyanobacteria forming intracellular calcium carbonates, Environ. Sci. Technol., 53, 12639–12647, https://doi.org/10.1021/acs.est.9b03982, 2019.

Mehta, N., Bougoure, J., Kocar, B. D., Duprat, E., and Benzerara, K.: Cyanobacteria accumulate Radium (226Ra) within intracellular amorphous calcium carbonate inclusions, ACS EST Water, 2, 616–623, https://doi.org/10.1021/acsestwater.1c00473, 2022a.

Mehta, N., Gaëtan, J., Giura, P., Azaïs, T., and Benzerara, K.: Detection of biogenic amorphous calcium carbonate (ACC) formed by bacteria using FTIR spectroscopy, Spectrochimica Acta Part A: Molecular and Biomolecular Spectroscopy, 278, 121262, https://doi.org/10.1016/j.saa.2022.121262, 2022b.

Mehta, N., Coutaud, M., Bouchez, J., van Zuilen, K., Bradbury, H. J., Moynier, F., Gorge, C., Skouri-Panet, F., and Benzerara, K.: Barium and strontium isotope fractionation by cyanobacteria forming intracellular carbonates, Geochimica et Cosmochimica Acta, 356, 165–178, https://doi.org/10.1016/j.gca.2023.07.014, 2023.

Mehta, N., Bradbury, H., and Benzerara, K.: Calcium isotope fractionation by intracellular amorphous calcium carbonate (ACC) forming cyanobacteria, Geobiology, 22, e12596, https://doi.org/10.1111/gbi.12596, 2024.

Milucka, J., Kirf, M., Lu, L., Krupke, A., Lam, P., Littmann, S., Kuypers, M. M., and Schubert, C. J.: Methane oxidation coupled to oxygenic photosynthesis in anoxic waters, ISME J, 9, 1991–2002, https://doi.org/10.1038/ismej.2015.12, 2015.

Monteil, C. L., Benzerara, K., Menguy, N., Bidaud, C. C., Michot-Achdjian, E., Bolzoni, R., Mathon, F. P., Coutaud, M., Alonso, B., Garau, C., Jézéquel, D., Viollier, E., Ginet, N., Floriani, M., Swaraj, S., Sachse, M., Busigny, V., Duprat, E., Guyot, F., and Lefevre, C. T.: Intracellular amorphous Ca-carbonate and magnetite biomineralization by a magnetotactic bacterium affiliated to the Alphaproteobacteria, The ISME Journal, 1–18, https://doi.org/10.1038/s41396-020-00747-3, 2020.

Oshkin, I. Y., Danilova, O. V., But, S. Y., Miroshnikov, K. K., Suleimanov, R. Z., Belova, S. E., Tikhonova, E. N., Kuznetsov, N. N., Khmelenina, V. N., Pimenov, N. V., and Dedysh, S. N.: Expanding characterized diversity and the pool of complete genome sequences of *Methylococcus* species, the bacteria of high environmental and biotechnological relevance, Front. Microbiol., 12, https://doi.org/10.3389/fmicb.2021.756830, 2021.

Otón, J., Pereiro, E., Pérez-Berná, A. J., Millach, L., Sorzano, C. O. S., Marabini, R., and Carazo, J. M.: Characterization of transfer function, resolution and depth of field of a soft X-ray microscope applied to tomography enhancement by Wiener deconvolution, Biomed. Opt. Express, BOE, 7, 5092–5103, https://doi.org/10.1364/BOE.7.005092, 2016.

Pamart, E., Benzerara, K., Fois, G. R., Viola, S., Chauvat, F., Cassier-Chauvat, C., and Chapon, V.: Exploring the potential of *Gloeomargarita* lithophora for radionuclides bioremediation, JOURNAL OF HAZARDOUS MATERIALS, 492, https://doi.org/10.1016/j.jhazmat.2025.138155, 2025.

Parks, D. H., Chuvochina, M., Rinke, C., Mussig, A. J., Chaumeil, P.-A., and Hugenholtz, P.: GTDB: an ongoing census of bacterial and archaeal diversity through a phylogenetically consistent, rank normalized and complete genome-based taxonomy, Nucleic Acids Res, 50, D785–D794, https://doi.org/10.1093/nar/gkab776, 2022.

Pettersen, E. F., Goddard, T. D., Huang, C. C., Couch, G. S., Greenblatt, D. M., Meng, E. C., and Ferrin, T. E.: UCSF Chimera-a visualization system for exploratory research and analysis, J Comput Chem, 25, 1605–1612, https://doi.org/10.1002/jcc.20084, 2004.

Ponce-Toledo, R. I., Deschamps, P., López-García, P., Zivanovic, Y., Benzerara, K., and Moreira, D.: An early-branching freshwater cyanobacterium at the origin of plastids, Current Biology, 27, 386–391, https://doi.org/10.1016/j.cub.2016.11.056, 2017.

Qin, W., Wang, C., Ma, Y., Shen, M., Li, J., Jiao, K., Tay, F. R., and Niu, L.: Microbe-mediated extracellular and intracellular mineralization: environmental, industrial, and biotechnological applications, Adv. Mater., 32, 1907833, https://doi.org/10.1002/adma.201907833, 2020.

Rivas-Lamelo, S., Benzerara, K., Lefèvre, C., Monteil, C., Jézéquel, D., Menguy, N., Viollier, E., Guyot, F., Ferard, C., Poinsot, M., Skouri-Panet, F., Trcera, N., Miot, J., and Duprat, E.: Magnetotactic bacteria as a new model for P sequestration in the ferruginous Lake Pavin, Geochemical Perspectives Letters, 5, 35–41, https://doi.org/10.7185/geochemlet.1743, 2017.

Safitri, A. S., Hamelin, J., Kommedal, R., and Milferstedt, K.: Engineered methanotrophic syntrophy in photogranule communities removes dissolved methane, Water Research X, 12, 100106, https://doi.org/10.1016/j.wroa.2021.100106, 2021.

Schewiakoff, W.: Uber einen neuen bakteriennähnlichen Organismus des Süßwassers, Habilitationsschrift, Heidelberg, 1893.

Sorrentino, A., Nicolás, J., Valcárcel, R., Chichón, F. J., Rosanes, M., Avila, J., Tkachuk, A., Irwin, J., Ferrer, S., and Pereiro, E.: MISTRAL: a transmission soft X-ray microscopy beamline for cryo nano-tomography of biological samples and magnetic domains imaging, J Synchrotron Rad, 22, 1112–1117, https://doi.org/10.1107/S1600577515008632, 2015.

Vantelon, D., Trcera, N., Roy, D., Moreno, T., Mailly, D., Guilet, S., Metchalkov, E., Delmotte, F., Lassalle, B., Lagarde, P., and Flank, A.-M.: The LUCIA beamline at SOLEIL, J Synchrotron Rad, 23, 635–640, https://doi.org/10.1107/S1600577516000746, 2016.

Waditee, R., Hossain, G. S., Tanaka, Y., Nakamura, T., Shikata, M., Takano, J., Takabe, T., and Takabe, T.: Isolation and functional characterization of Ca^{2+}/H^{+} antiporters from Cyanobacteria, J. Biol. Chem., 279, 4330–4338, https://doi.org/10.1074/jbc.M310282200, 2004.

Wan, J., Ji, R., Liu, J., Ma, K., Pan, Y., and Lin, W.: Biomineralization in magnetotactic bacteria: From diversity to molecular discovery-based applications, Cell Reports, 43, https://doi.org/10.1016/j.celrep.2024.114995, 2024.

Wong, T. K. F., Ly-Trong, N., Ren, H., Baños, H., Roger, A. J., Susko, E., Bielow, C., Maio, N. D., Goldman, N., Hahn, M. W., Huttley, G., Lanfear, R., and Minh, B. Q.: IQ-TREE 3: Phylogenomic inference software using complex evolutionary models, 2025.

Yang, T., Teske, A., Ambrose, W., Salman-Carvalho, V., Bagnell, R., and Nielsen, L. P.: Intracellular calcite and sulfur dynamics of *Achromatium* cells observed in a lab-based enrichment and aerobic incubation experiment, Antonie van Leeuwenhoek, 112, 263–274, https://doi.org/10.1007/s10482-018-1153-2, 2019.

Zhang, K., Tang, C.-S., Jiang, N.-J., Pan, X.-H., Liu, B., Wang, Y.-J., and Shi, B.: Microbial-induced carbonate precipitation (MICP) technology: a review on the fundamentals and engineering applications, Environ Earth Sci, 82, 1–33, https://doi.org/10.1007/s12665-023-10899-y, 2023.